ELSEVIER

Advances in Water Resources 24 (2001) 1015–1036

Advances in Water Resources

www.elsevier.com/locate/advwatres

Temporal scales of rainfall–runoff processes and spatial scaling of flood peaks: space–time connection through catchment water balance

Chatchai Jothityangkoon, Murugesu Sivapalan *

Department of Environmental Engineering, Centre for Water Research, University of Western Australia, 35 Stirling Highway, Crawley, WA 6009, Australia

Received 24 July 2000; received in revised form 28 February 2001; accepted 11 March 2001

Abstract

This paper investigates the scaling behaviour of annual flood peaks, exhibited through what is taken to be a power law relationship between mean annual flood and catchment size, $E[Q_p] = cA^{\theta}$. We also study the dependence on catchment size of the coefficient of variation of annual flood peaks, $CV[Q_p]$. We attempt to interpret these relationships in terms of the interactions between the land surface and the atmosphere – in particular, the effects of temporal variability of rainfall (within-storm patterns, multiple storms and seasonality) and runoff processes (overland flow, subsurface flow and channel flow). The spatial scaling of flood peaks, as expressed by the coefficients c, θ and CV, has been analysed based on, initially, simulated runoff fields produced by a simple linear rainfall–runoff model for hypothetical catchments, and later by a more realistic, distributed model for an actual catchment in the semi-arid, south-west of Western Australia. It is found that the main controls on c and θ are runoff processes, soil depth and mean annual rainfall, with additional controls on c including temporal rainfall variability, the underlying water balance, and the spatial variability of rainfall. Runoff generation at catchment scales can be specified as being fast or slow according to a relative catchment travel time. The scaling exponent θ is high and almost constant with A for slow catchments, where deep soils combined with low annual rainfall leads to domination by subsurface flow. Conversely, θ is lower in fast catchments, where shallow soils combined with high annual rainfall leads to dominance by surface runoff processes with relatively short travel times. The interaction between within-storm patterns and fast runoff processes is the important control on c, clearly shown in small catchments, while multiple storms and seasonality are crucial in large catchments. The presence of multiple runoff processes with a broad spectrum of time scales leads to an increase of $CV[Q_p]$, as does the introduction of spatial variability of rainfall.

Keywords: Rainfall variability; Spatial scaling; Flood peaks; Water balance; Runoff processes; Runoff modelling; Western Australia

1. Introduction

The dependence of annual flood peaks on catchment size forms the basis of many empirical methods for the estimation of floods in ungauged basins. This spatial scaling behaviour also provides a natural framework to understand the physical controls of regional variations in annual flood peaks. Empirical analyses of regional flood frequency in catchments around the world has revealed that the relationship between the annual flood peaks of a given return period, Q_T, and catchment area, A, can be framed in terms of the power function relationship,

$$Q_T = c(T)A^{\theta(T)}, \tag{1}$$

where the constant c and a characteristic exponent θ are parameters which, in general, are functions of the return period T. If θ remains constant and independent of T in a region, the annual flood peaks are said to obey *simple scaling* and the catchments in the region are said to be "homogeneous". If, on the other hand, θ changes with T, then flood peaks are said to obey *multiscaling*. More importantly, the scaling exponents θ contain key physical information about catchment rainfall–runoff processes and how these may change with increasing catchment size [4,6,14,17]. Huang and Willgoose [8] gave a physical interpretation for θ as a measure of the

* Corresponding author. Tel.: +61-9-380-2320; fax: +61-9-380-1015.
E-mail address: sivapalan@cwr.uwa.edu.au (M. Sivapalan).

0309-1708/01/$ - see front matter
PII: S0309-1708(01)00044-6

rainfall to runoff transformation, and in particular, the degree to which water is retarded, filtered or diminished by the catchment.

In this paper we investigate the process controls on the relationship between observed mean annual peak floods ($E[Q_p]$) and A for catchments in the Collie River Basin, south-west of Western Australia. Empirical evidence from this catchment indicates that $E[Q_p]$, expressed in depth units or mm/day, remains almost constant with increasing catchment size; in other words, the exponent θ is close to 0. However, in previous studies on other catchments, θ has been found to be about -0.33 in the central Appalachian region of the eastern United States [14,17], about -0.25 in Austrian catchments [2], in the range of -0.1 to -0.3 for a snowmelt generated region in USA [4], and in the range -0.1 to -0.4 in other regions such as Australia and New Zealand [11–13]. These observations naturally lead to the question, what are the process controls, which cause the constancy of the exponent θ in Western Australian catchments? What are the causes of such differences of θ between different regions? This is the subject of this paper.

Many recent papers on the scaling of regional flood frequency have focussed their efforts towards understanding the process controls on the variation with catchment size of the mean, $E[Q_p]$, and the coefficient of variation, $CV[Q_p]$, of the flood peaks within a geographical region [2,14]. Robinson and Sivapalan [14] showed that the interactions between time scales, namely between rainfall duration and catchment response time, lay at the heart of these process controls. The way that catchment response time varies with catchment area depends on the relative dominance of hillslope response, channel hydraulic response, and network geomorphology [16]. A consequence of this is that, as shown by Robinson and Sivapalan [15], the observed log–log linearity of the $E[Q_p]$ versus A relationship may be a result of a "resonance" between the increasing catchment response time and the changing time scales associated with rainfall variability. At small catchment scales, within-storm patterns of rainfall variability are important, while at large catchment scales, longer time scales such as seasonality are important. This then gives rise to a phenomenon which can be described as representing a space to time connection – a spatial scaling behaviour which is generated by the interactions in the time domain between rainfall and runoff processes, and provides further motivation for the work presented in this work.

In addition to the above reasons, the space–time connection can be modified, sometimes significantly, by the non-linearity of the rainfall–runoff processes, as observed by Blöschl and Sivapalan [2] and Robinson and Sivapalan [15]. All of the papers cited above used, essentially, spatially lumped models and did not explicitly include spatial variability of rainfall or the branched structure of stream network. Using the hypothesis of self-similarity, or scaling invariance, in the spatial variability of rainfall and channel network properties, Gupta et al. [7] developed a theoretical modelling framework, which indicated that the scaling exponents of flood peaks can be computed by combining the scaling of exponents relating to the spatial variability of rainfall intensity and of channel network structure.

This paper is an extension of, and has been motivated by, the previous work of Robinson and Sivapalan [14] and Robinson and Sivapalan [15]. Firstly, in addition to dealing with multiple time scales of variability of the rainfall inputs, we also allow for the presence of multiple time scales of variability of runoff processes (multiple pathways), permitting multiscale interactions between atmospheric and land surface processes. Secondly, in this case we use a distributed rainfall model, thus allowing for spatial variability of rainfall and landscape properties to be explicitly incorporated. Thirdly, in this paper we utilise a long-term water balance model, previously developed and well-tested in the Collie River Basin, to underpin the prediction of floods, and explicitly incorporating the effects of antecedent conditions. This connection to the underlying water balance is important for the slow catchments of Western Australia, and is a major extension of previous work.

In this context, Fig. 1(a) formally presents our hypothesis on what are the possible controls on the spatial variability of flood peaks: (i) temporal variability of rainfall intensity (this was studied previously by Robinson and Sivapalan [14,15]), (ii) variability of runoff processes in terms of the multiplicity of pathways that water takes to arrive at the catchment outlet (this is the main extension in this paper), and (iii) the spatial variability of climate, soil and vegetation (this is also included in a simple manner). Similarly, Fig. 1(b) illustrates our view as to how the observed spatial scaling of flood peaks may be connected to the space–time variability of rainfall–runoff processes through the underlying catchment water balance (and motivates the need for a realistic long-term rainfall–runoff model) and the associated stream network geomorphology. The catchment partitions the rainfall fields, which vary in space and time, into runoff, evaporation and soil moisture storage (also space–time fields), which can be expressed through the water balance equation. This equation incorporates the memory inherent to the catchment system, and its effect of individual flood peaks, through the antecedent runoff and soil moisture conditions prior to the storm event. The catchment responds to a single event depending on the memory embedded in the water balance, which accumulates the net effect of many previous storm events, thus providing a long-term causal link to the shape of the flood frequency curve [5,15].

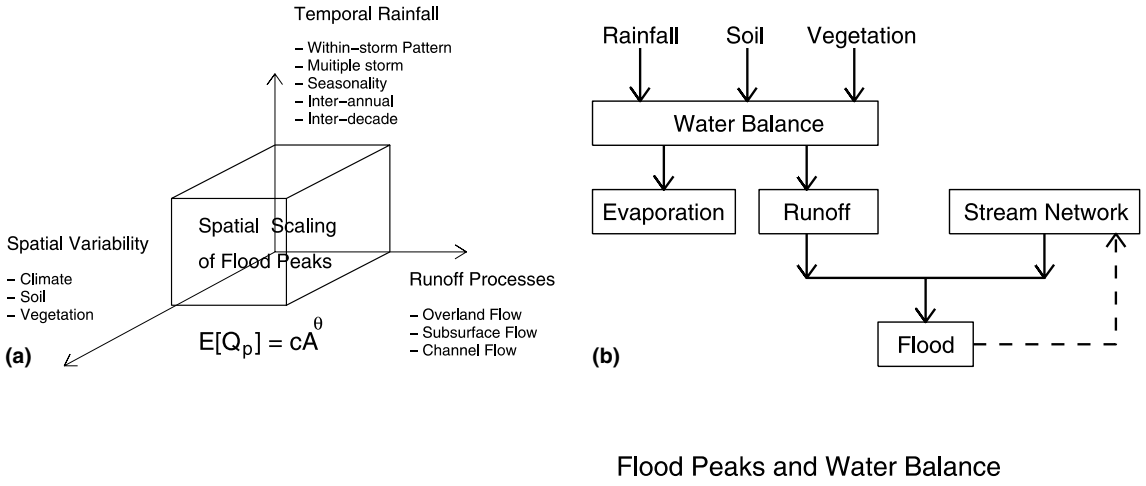

Fig. 1. (a) The three main factors which impact on the spatial scaling of flood peaks; (b) schematic plot showing connection between rainfall–runoff processes and flood peaks, through catchment water balance and stream network.

Furthermore, the spatial variability of flood peaks in a large catchment is constrained by the topology of the river channel network. Runoff or flood peak at any specified point in the network is not only controlled by the local partitioning of rainfall into runoff, but in fact by the water balance associated with the entire upstream area contributing up to that point. The change of magnitude of flood peaks with increasing catchment area is the net effect of flood intensification through hillslope contributions in the downstream direction, and attenuation of the resulting flood waves due to friction effects, adding to the effects of the spatial variability of rainfall and network geomorphology. It should be noted that, from a long-term perspective, the effect of network geomorphology is not a one-way control on the spatial variability of flood peaks. The channel network itself is carved by the repeated action of floods, and network geomorphology is thus a consequence of the spatial variability of flood peaks. However, this feedback is ignored here.

The aim of the paper is to systematically investigate the space–time connections between temporal scales of rainfall–runoff processes and the resulting spatial scaling behaviour of flood peaks. We do this initially by using a simple, runoff generation model at the hillslope or sub-catchment scale, and later a distributed, combined hillslope water balance and network flood routing model. This distributed rainfall–runoff model is applied to actual catchments with climatic and soils data from catchments in Western Australia and Queensland, to investigate the effects of the underlying water balance on the scaling behaviour of annual maximum flood peaks. The results from many different simulations using the model, with different combinations of climate, soil and runoff processes, are then interpreted with a view to gaining insights into the connections between flood frequency scaling and underlying water balance.

2. Scaling of flood peaks in a hypothetical catchment

2.1. Temporal scales of rainfall and spatial scaling of flood peaks

Robinson and Sivapalan [15] investigated the role of interactions between rainfall time scales and time scales of catchment response on the magnitudes and spatial scaling of flood peaks. They developed an empirically based rainfall model, which could incorporate different temporal scales of variability of rainfall intensity (within-storm patterns, between-storm interactions, and seasonality). Rainfall time series generated by this model were combined with a simple linear model of a hypothetical catchment response, in which runoff is a linear function of storage and there is no evapotranspiration,

$$\mathrm{d}s/\mathrm{d}t = i(t) - q(t), \tag{2}$$

$$q(t) = s(t)/t_c, \tag{3}$$

where $s(t)$ is water storage in the catchment, $i(t)$ is the rainfall intensity, $q(t)$ is the rate of streamflow at the catchment outlet, and t_c is the mean catchment response time.

To investigate the nature of the interactions between rainfall time scales and catchment response time, Robinson and Sivapalan [15] considered five rainfall scenarios, ranging from the most comprehensive structure typical of south-west Western Australia, down to the most simple. Fig. 3 presents in a schematic manner, examples of rainfall time series generated by the rainfall model for each of these scenarios. Readers should note the symbols used to represent each of the rainfall scenarios, as these will be used throughout the paper.

The rainfall time series, for the various scenarios, were combined with the linear model of catchment response presented above, to derive the flood frequency curves for hypothetical catchments, and then to estimate the mean annual flood, $E[Q_p]$, and the coefficient of variation, $CV[Q_p]$, of annual flood peaks. To provide motivation for the rest of the paper, these are reproduced from Robinson and Sivapalan [15], with some adaptation, in Figs. 2(a) and (b). Robinson and Sivapalan [15] found that the combined effects of within-storm patterns, multiple storms, and seasonality have an important bearing on the spatial scaling of flood peaks. For example, in a fast catchment (low t_c) within-storm patterns have the biggest impact on flood peaks, while in a slow catchment (large t_c) multiple storms and seasonality are important (Fig. 2(a)). The relationship between $E[Q_p]$ versus t_c in Fig. 2(a) can be converted to one between $E[Q_p]$ and catchment area A by using an empirical relationship between t_c and A, such as $t_c = 0.28A^{\beta}$. The results are shown in Fig. 2(b). The contention of Robinson and Sivapalan [15] was that the observed log–log linearity in the relationship between t_c and A is a result of the interactions between catchment response time t_c and the time scales of rainfall variability associated with within-storm patterns, multiple storms and seasonality.

However, in the previous work just described above, the multiple time scales of variability associated with catchment runoff responses, as can be seen from the work of Robinson et al. [16], and also the effects of nonlinearity of rainfall–runoff response were not considered. Both are important for the extension of the scaling ideas to real catchments, and for a comparison of the behaviour of catchments in different climatic and hydrologic settings. This paper goes some way towards fulfilling this need.

2.2. Temporal scales of runoff processes and spatial scaling of flood peaks

To gain further insights into the issue of space–time connections in catchment responses, we extend the simple linear model of the hypothetical catchment with additional complexity. We separate both the catchment response time t_c and the water storage s of the catchment into two components. The first pair, t_h and s_h, are the hillslope travel time and soil water storage, respectively, while the second pair, t_n and s_n, are, respectively, time of travel and water storage over the catchment's stream network.

The simple linear model previous described through Eqs. (2) and (3) can then be generalised to:

$$ds_h/dt = i(t) - q_h(t), \tag{4a}$$

$$q_h(t) = s_h(t)/t_h. \tag{4b}$$

$$ds_n/dt = q_h(t) - q_n(t), \tag{5a}$$

$$q_n(t) = s_n(t)/t_n, \tag{5b}$$

where q_h is runoff from hillslope and q_n is channel flow at the catchment outlet. The hillslope runoff process in (4a) and (4b) can be identified as subsurface flow. We assume that t_h is independent of catchment size, and the relationship between t_n and catchment size A is assumed as follows [15]:

$$t_n = 0.28A^{\beta}, \tag{6}$$

where t_n is in hours, A is in km^2, and $\beta = 0.5$. Following Robinson et al. [16], we further assume that hillslope and channel network processes are independent, and occur in series so that the total catchment storage and total residence time would be arithmetic summations of the corresponding hillslope and network components.

The linear model given by (4a)–(6), was combined with the synthetic time series of rainfall from the rainfall

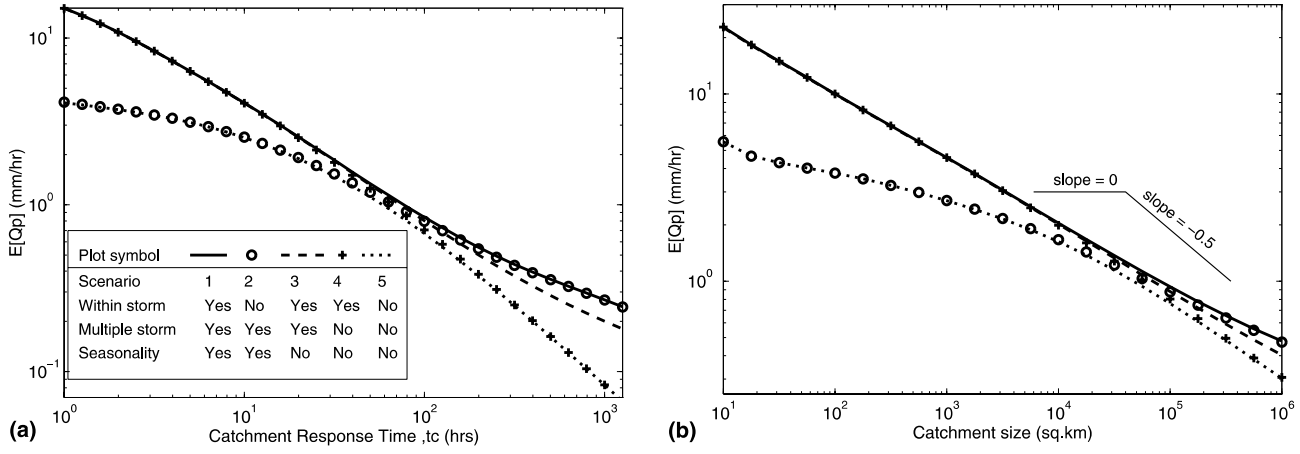

Fig. 2. Mean annual flood peak resulting from five rainfall scenarios, (a) $E[Q_p]$ as the function of catchment response time t_c, (b) $E[Q_p]$ as a function of catchment size A.

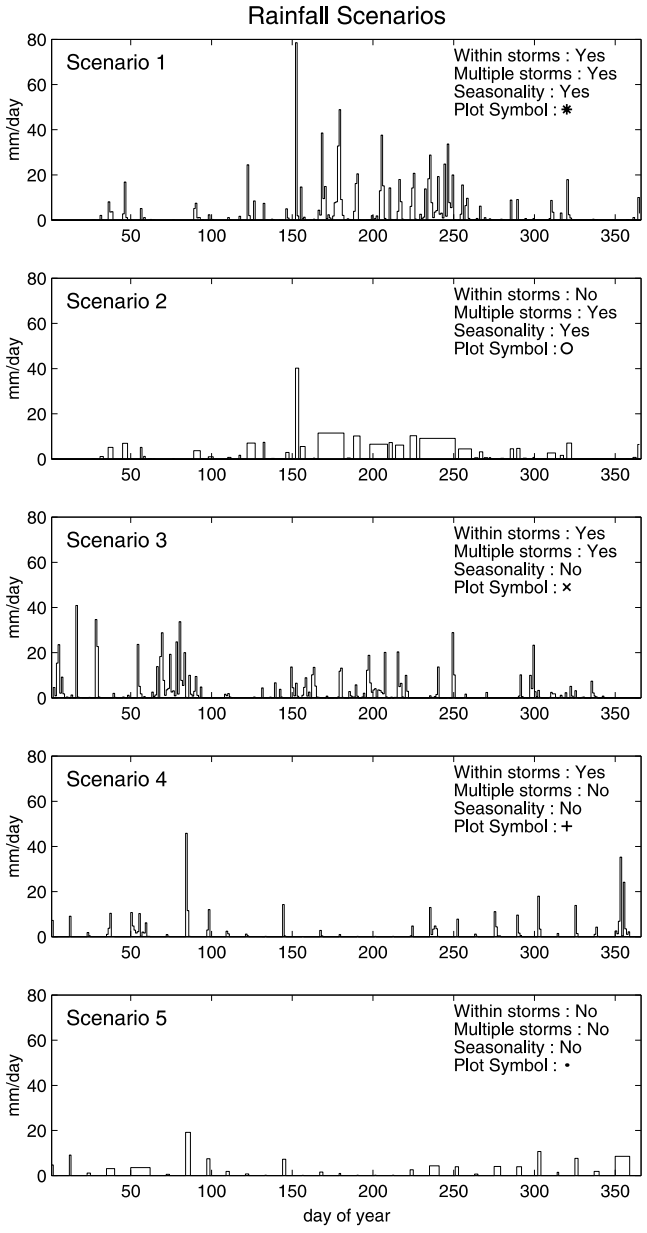

Fig. 3. Schematic descriptions of five different scenarios temporal rainfall variability.

model developed by Robinson and Sivapalan [15], for the five rainfall scenarios described in Fig. 3. This produced an annual maxima series of flood peaks, 100 years long, and was used to estimate $E[Q_p]$ for a range of catchment sizes. The simulation results, for different values of the hillslope response time t_h, are shown in Fig. 4. Fig. 4(a) presents the variation of $E[Q_p]$ with catchment are A for each of the five rainfall scenarios, and for $t_h = 1$, 20, and 100 h. Firstly, $t_h = 1$ h signifies low retardation or a rapid hillslope runoff response, hence catchment response is dominated by channel response, and results similar to Fig. 2(b) are obtained. Increase of t_h leads to an increase of the scaling exponent θ, in the power law relationship given by (1), and a decrease of the absolute magnitude of $E[Q_p]$, and the coefficient c in (1). In small catchments, the effect of within-storm patterns becomes less important as t_h increases. On the other hand, in large catchments the effects of multiple storms and seasonality become more important when t_h increases (Fig. 4(a)).

The next set of simulations is designed to investigate the effects of multiple time scales, which may be present in the hillslope response. We assume that the catchment may exhibit hillslope responses which operate at all three time scales of $t_h = 1$, 20, 100 h, but in different proportions. In the first case, the proportions are 85%, 15% and 0%, respectively, and is dominated by the fast response process of $t_h = 1$. In the second case, the proportions are 0%, 15% and 85%, respectively, thus it is dominated by slow responses, i.e., $t_h = 100$ h. Fig. 4(b) presents the resulting $E[Q_p]$ versus A relationship for these two categories of hillslope responses exhibiting multiple time scales, for the five rainfall scenarios described before. We find that, for small catchments, the reduction in the proportion of fast responses, i.e., $t_h = 1$ h, from 85% to 15 % causes a reduction of $E[Q_p]$ but does not affect θ. Compare this to the case when the fraction of $t_h = 1$ h was 0, in which case $E[Q_p]$ decreases further, and the exponent θ is effectively 0. This result shows that even a small proportion of fast hillslope runoff process ($t_h = 1$) can interact with within-storm patterns of rainfall variability, as if to produce a resonance effect, and is enough to produce a higher $E[Q_p]$ and lower θ in small catchments. The situation is reversed, but not quite as strongly, for large catchments with the increase in the proportion of slow response processes, i.e., $t_h = 100$ h.

The simple runoff model above can be improved further to incorporate a third runoff process, namely saturation overland flow (q_o). This overland flow can be assumed to occur if water storage exceeds the storage capacity (S_b),

$$q_o = s_h(t) - S_b \quad \text{if } s_h(t) > S_b, \tag{7a}$$

$$q_o = 0 \quad \text{if } s_h(t) < S_b. \tag{7b}$$

Fig. 5 presents the $E[Q_p]$ versus A relationship which results when all three runoff processes operate, for three different subsurface response times t_h (1, 20 and 100 h), and bucket capacity, $S_b = 100$ mm. The simulations were repeated as before for the five rainfall scenarios. For $t_h = 1$ and 20 h, the shape of the $E[Q_p]$ versus A relationships in Fig. 5 is similar to that in Fig. 4(a) since, due to the short residence time in the store in both cases, runoff is dominated by subsurface flow. However, when $t_h = 100$ h, $E[Q_p]$ becomes larger for small catchments. This is because, due to the slow subsurface flow response, the store is able to become full sooner, and saturation excess overland flow begins to dominate $E[Q_p]$.

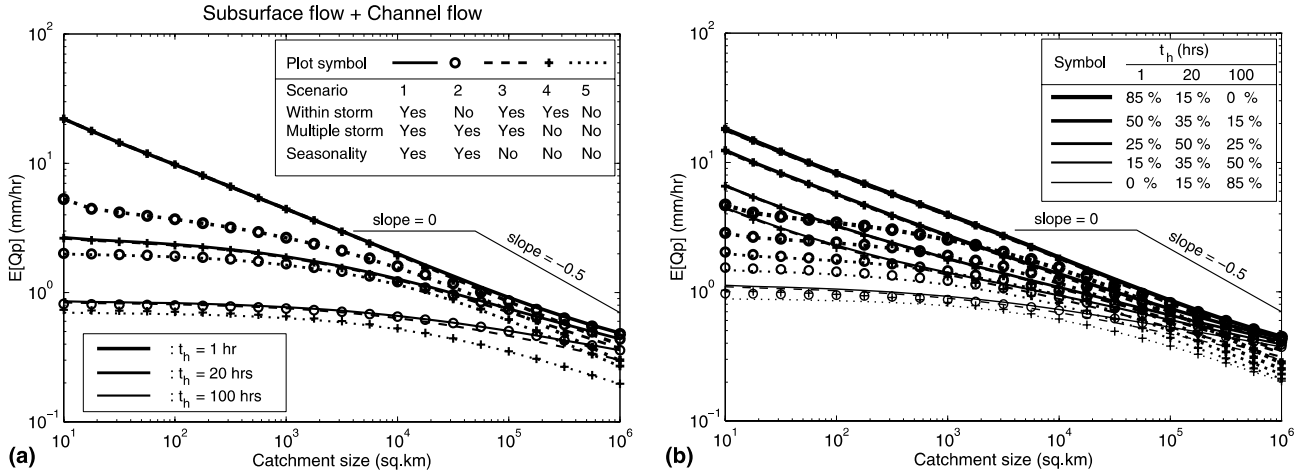

Fig. 4. Mean annual flood peak resulting from five rainfall scenarios, using simple model consisting of two runoff processes: subsurface flow and channel flow, (a) $E[Q_p]$ as a function of A for three hillslope response times ($t_h = 1$, 20 and 100 h), (b) $E[Q_p]$ as the function of A for five different combinations of hillslope response times.

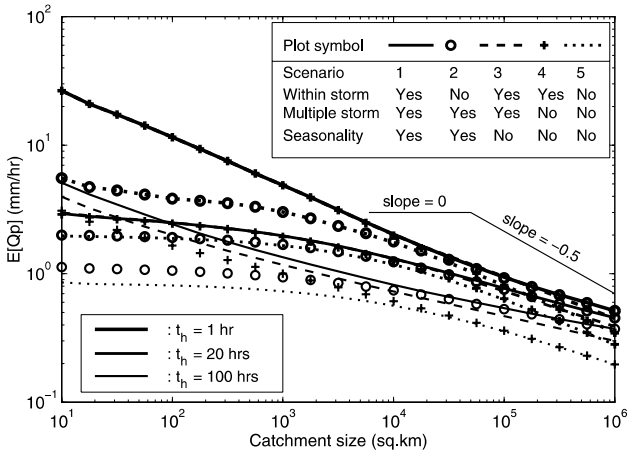

Fig. 5. Mean annual flood peak resulting from five rainfall scenarios, using simple model consisting of three runoff processes: subsurface flow, overland flow and channel flow, $E[Q_p]$ as a function of A for three hillslope response times ($t_h = 1$, 20 and 100 h).

Focussing on the effect of different rainfall scenarios, it is interesting to note when saturation excess overland flow is dominant (i.e., $t_h = 100$ h) not only within-storm patterns but even multiple storms and seasonality make a substantial impact on $E[Q_p]$ and its scaling behaviour, for small catchments. This is because the interactions between successive storms and seasonality affect saturation excess overland flow through their control on the rate of accumulation of water in the hillslope store.

The tendency for $E[Q_p]$ to decrease with increasing catchment size, as shown in Figs. 4 and 5, has been observed in actual catchments, but with a large amount scatter in small catchments [2]. Blöschl and Sivapalan [2] have explained that this tendency arises from the fact the area dependence of $E[Q_p]$ is controlled by a combination of the many different rainfall–runoff processes which may be present in the region, operating under different hydrologic regimes.

3. A distributed flood peak model for an actual catchment

The models described above cannot be used to estimate flood frequency scaling relationships in actual catchments because (i) they ignore evapotranspiration, and (ii) they ignore spatial variability of rainfall and catchment properties. Evapotranspiration is an important component of water balance, especially in semi-arid catchments where it may be as high as 90% on an annual basis. Similarly, spatial heterogeneity cannot be ignored in any study that aims to investigate spatial scaling behaviour of flood peaks. Thus we would require a distributed model of the complete water cycle for realistic simulation of regional flood frequency.

The distributed model we use here divides the catchment into a number of subcatchments based around the stream network, with each stream reach being associated with a subcatchment of known area. Runoff is generated within the subcatchments, based on an appropriate water balance model, and the runoff generated is then routed down the stream network. The distributed modelling framework can be presented in terms of the following mass balance equation for a particular stream reach [5]:

$$\frac{dV}{dt} = -q(i,t) + \sum q(j, t - \Delta t) + r(i,t)a(i). \quad (8)$$

Here, $V(i,t)$ denotes the volume of water stored in link i at time t, and $q(i,t)$ is the space–time runoff field representing the discharge across any reach i in the channel network, and the summation of $q(j, t - \Delta t)$ is for discharges from all links j which join i at its upstream end.

The term $r(i,t)a(i)$ represents the rate of runoff contribution into the link i from the adjacent subcatchment, during a chosen time interval $(t-\Delta t, t)$, where $a(i)$ denotes the area of the subcatchment associated with reach i, and $r(i,t)$ is the rate of runoff generation per unit area over this land area.

The hillslope contributions to the stream network are a result of rainfall partitioning based on the water balance on the individual subcatchments. This rainfall partitioning (hillslope water balance) is represented by the following:

$$\frac{\mathrm{d}s}{\mathrm{d}t} = p(i,t) - e(i,t) - r(i,t), \tag{9}$$

where $s(i,t)$ is the soil–water storage, $p(i,t)$ is rainfall intensity, and $e(i,t)$ is rate of evapotranspiration, estimated for those hillslopes/subcatchment directly contributing to link i. Details about the hillslope water balance model and the network routing model used in this paper are presented in the following two sections.

3.1. Hillslope model of runoff generation and water balance

To estimate $r(i,t)$ in actual catchments, we use the subcatchment scale water balance model proposed by Jothityangkoon [9] and Jothityangkoon et al. [10]. This conceptual model is based on a configuration of assumed soil–water stores, and was constructed using a "downward or top–down" approach which helped identify appropriate levels of complexity for making predictions at different time scales. In the present case a model with a daily time step is used, which is justified for the particular catchments used here, due to their generally slow runoff response.

The chosen model considers both subsurface flow, q_{ss}, and saturation excess overland flow, q_{se}, in estimating the total runoff $r(i,t)$. Evapotranspiration includes both bare soil evaporation, e_b, and transpiration, e_v. Subsurface runoff is a function of soil water storage (s) and a threshold water holding capacity (s_f), through an assumed non-linear storage–discharge relationship (using parameters a and b),

$$q_{ss} = \left[\frac{s - s_f}{a}\right]^{1/b}, \quad \text{if } s > s_f, \tag{10a}$$

$$q_{ss} = 0, \quad \text{if } s < s_f. \tag{10b}$$

The rates of bare soil evaporation and transpiration are assumed to be linear functions of s, the soil–water storage capacity, S_b, canopy density M, potential evaporation rate e_p (which is specified on a daily basis) and plant transpiration efficiency, k_v. Details of these parameterisations are given in [9,10] and are not repeated here.

All of the parameters of this model were estimated a *priori*, as a non-calibrated model is appropriate for the extrapolations involved in scaling. The model uses a probability distribution of soil depths, based on surveyed soil depths in the study catchments. These are used to estimate bucket capacities, S_b, for each subcatchment. The parameters a and b in (10a) and (10b) are estimated based on extensive recession analyses carried out on observed streamflows. The parameter M is estimated a *priori* based on vegetation cover information, and the parameter k_v is fixed at a value of 1.2.

3.2. Routing model

The routing model is based on a constant stream velocity algorithm developed by Viney and Sivapalan [18], which is consistent with the application of (8). It assumes that the runoff volume from upstream subcatchments enters the stream channel uniformly in time throughout the day, and that runoff from the adjacent hillslopes enters the stream uniformly in time and uniformly in space along the channel length. Using a single optimisable parameter, stream velocity, assumed constant in space and time, the model calculates the volume of runoff passing out of each subcatchment in each time step, and the in-stream runoff volume that has not yet reached the subcatchment outlet. This model, unlike the Muskingum–Cunge model and the kinematic wave model, does not require knowledge of channel cross-sections, and does not introduce any other unknown parameters, and is parsimonious. We realise that this approach is too simplistic and may not adequately capture possible attenuation of flood waves. It was chosen because in the study catchment the main attenuation happens within the hillslopes because of the large residence times of hillslope runoff processes, and the attenuation in the stream network is comparatively small.

3.3. Estimation of annual flood peaks

Provided the necessary input data and parameterisations, (8) and (9) can be solved over the entire stream network-subcatchment system, yielding the space–time discharge field $q(i,t)$ for every link i within the large river network at any time t. In this study, we focus our attention to the spatial field of peak flow defined as:

$$Q_p(i) = \max_{0 \leqslant t \leqslant \tau} q(i,t), \tag{11}$$

where $\tau = 1$ year; $Q_p(i)$ represents the annual maximum peak flow in link i.

4. Simulation results and discussion

4.1. Parameter estimation and model time step

The distributed rainfall–runoff model described above has a number of parameters, which need to be

estimated from observed streamflows, catchment characteristics and the stream network, with no calibration. The method of estimation of these parameters has been described in detail by Jothityangkoon [9] and Jothityangkoon et al. [10] . For the purpose of this flood study, we estimated these parameters from the Collie River Basin (2545 km^2) in Western Australia. Fig. 6 shows the location of the Collie River Basin and its stream network, Table 1 summarises its physical and climatic characteristics, and Table 2 presents the estimated model parameter values relating to both the hillslope water balance and stream network routing properties. To investigate the effects of different climatic and catchment characteristics, we estimated a second set of hillslope water balance parameters from the Broken River catchment (41 km^2) in Queensland. Details of the physical and climatic characteristics of this catchment are described in [1,3], and are summarised in Table 1.

The distributed rainfall–runoff model we use here is a slightly simplified version of the daily water balance model for the Collie River Basin developed by Jothityangkoon [9] and Jothityangkoon et al. [10]. We continue

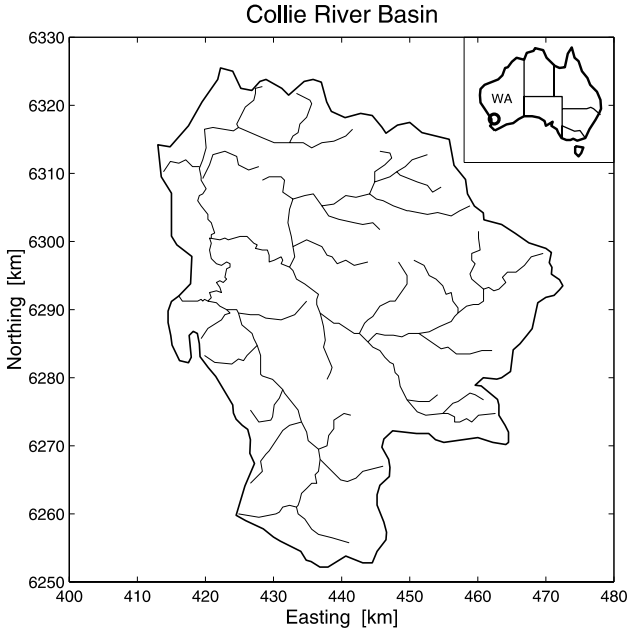

Fig. 6. Location of the Collie River Basin, and its stream network.

Table 1
Summary of physical and climatic characteristics of the Collie catchment and Broken River

	Collie, WA	Broken, QLD
Period of record	1983–1993	1965–1979
Catchment area (km^2)	2545	41
Altitude (m AHD)	200–350	750–1000
Annual rainfall (mm)	540–1160	2100
Annual runoff (mm)	5–50	1000
Annual pan evaporation (mm)	1400–1600	1560

Table 2
List of parameters for the space–time flood peak model, applied to Collie catchment, Western Australia and Broken River catchment, Queensland

Parameters	Collie, WA	Broken, QLD
(1) Hillslope water balance model		
Model structure		
Number of serial buckets	20	6
Storage–discharge relationship		
a (mm$^{0.5}$ day$^{0.5}$)	15	30
b	0.5	0.5
Soil properties		
ϕ	0.4	0.4
f_c	0.16	0.16
Mean S_b (mm)	1213	922
Min–max S_b (mm)	98–4207	130–1800
Vegetation		
M	0.7	0.6
k_v	1.2	1.0
Interception (%)	10	10
(2) Routing model		
Number of subcatchments	116	–
Channel flow velocity (km/day)	15	–

to use the model with a daily time step, although it is reasonable to think a model with a shorter time step may be required for flood calculations. To demonstrate the adequacy of a daily model, we present the observed flood frequency curves for the Salmon catchment (0.81 km^2), which is a small subcatchment located downstream of the main outlet of the Collie catchment. Fig. 7 shows two flood frequency curves, plotted using common units, but estimated from observed daily and

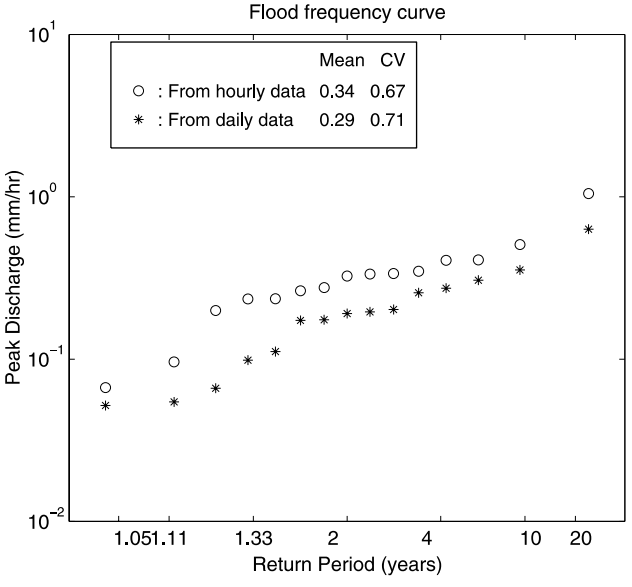

Fig. 7. Comparison of flood frequency curves estimated from observed hourly and daily flow data, Salmon catchment.

hourly peak flows. Clearly, the flood frequency curve estimated from daily flows is slightly lower than that obtained from hourly flows, but the shapes are similar. The Salmon catchment, consisting of deep soils, can be classified as a slow catchment [15], a consequence of which is that differences of flood peaks between the daily and hourly flood peaks are small, suggesting that it does not recognise the effects of variability of rainfall and infiltration processes at time scales less than daily. Since we are only interested in investigating spatial scaling behaviour of flood peaks, this suggests that a daily time step is still acceptable for this catchment. The daily model, on the other hand, has the advantage that the computational burden is very small even for multi-decadal simulations of flood frequency on a large stream network.

4.2. Synthetic generation of peak flow fields

The simulation process consists of four main steps: (i) generate five sets of rainfall time series representing the five rainfall scenarios (Fig. 3), with parameters estimated from observed rainfall data; (ii) generate space–time fields of runoff volumes, using the hillslope water balance model, for each of the above rainfall time series; (iii) route the generated runoff volumes, along stream network, to the catchment outlet and (iv) calculate annual flood peaks and annual water yields from each of the subcatchments. This process is repeated for each of the five rainfall scenarios.

Since our work focusses on the connection between temporal scales of rainfall–runoff processes and spatial scaling of flood peaks, spatial variabilities of rainfall and catchment characteristics are initially excluded. In other words, we initially use just one set of parameters and climatic inputs for all the subcatchments.

To investigate the effects of different combinations of multiple runoff processes or pathways, the application of the rainfall–runoff model is carried out for four different runoff process groupings: Group (i) channel flow only; Group (ii) overland flow and channel flow; Group (iii) subsurface flow and channel flow and Group (iv) subsurface and overland flow followed by channel flow. This is achieved by switching off the appropriate process in the running of the more complete model presented before. The first group, channel flow only, represents the so called "parking lot" or "very fast" catchment, where channel flow is the dominant process, and the model assumes that all of the rainfall is converted to runoff, instantaneously flowing into stream network, and with no losses to evaporation. In Group (ii), saturation excess overland flow is generated when the stores are filled by the incoming rainfall, subsurface flow is eliminated by the setting the storage–discharge parameter a to 0. In Group (iii), only subsurface flow is allowed, by setting the bucket capacities, S_b, to very large values. Finally, in Group (iv), all runoff and evaporation processes are assumed to occur naturally and simultaneously when the right conditions are satisfied.

To examine the effects of climate and catchment characteristics on the flood peaks, we repeat the above simulations (namely, five rainfall scenarios, for each of four groups of runoff combinations) for three different study cases. For Case I, the climatic input data and catchment parameters are estimated from the Collie catchment, Western Australia. Case II is similar to the Case I, except that the climate data are obtained from the Broken River catchment, in Queensland. For Case III, we use only the stream network from the Collie catchment, with the remainder of catchment characteristics and climatic inputs taken from the Broken River catchment.

4.3. Simulation results

The results of the simulations are presented in terms of the following signatures: (i) plots of mean annual maximum flood peaks $E[Q_p]$ versus catchment area A; (ii) the associated scaling exponent θ and coefficient c (Eq. (1)); (iii) plots of the coefficient of variation $CV[Q_p]$ versus A; (iv) plots of the mean annual water yield (total annual volume) versus A. The results from these simulations are presented next, along with a discussion of the insights they give to the issue of flood frequency scaling.

4.3.1. Case I: Collie catchment

Fig. 8(a) presents the $E[Q_p]$ versus A variation for the five rainfall scenarios, for the Group (i) runoff process, namely channel flow only. Here the scaling exponent θ decreases with increasing catchment size from about 0 to -0.5. This is identical to what one would expect in fast catchments [15]. For small catchments, removal of within-storm patterns (scenarios 2 and 5) significantly reduces the magnitudes of $E[Q_p]$ and thus c, but this effect is less important for large catchments. Similar results were also obtained for the hypothetical catchment, as shown in Fig. 2(b), except that θ was almost constant there. Further, we also see a slight decrease of $CV[Q_p]$ with increasing catchment size (Fig. 8(b)). The reduction of $E[Q_p]$ due to the removal of within-storm patterns appears to be connected to the increase of $CV[Q_p]$, in comparison to the other rainfall scenarios, noting that $CV[Q_p]$, is the ratio of standard deviation to the mean, $E[Q_p]$.

The results for Group (ii) runoff processes, namely combination of saturation excess overland with channel flow, are presented in Fig. 9. Compared to the case of channel flow alone (Fig. 8), the main difference is the reduction of $E[Q_p]$ by about an order magnitude, an increase of $CV[Q_p]$ from about 0.4 to about 1.0, and the reduction of annual water yield from 100% to below 2% of annual rainfall. The most obvious reason is

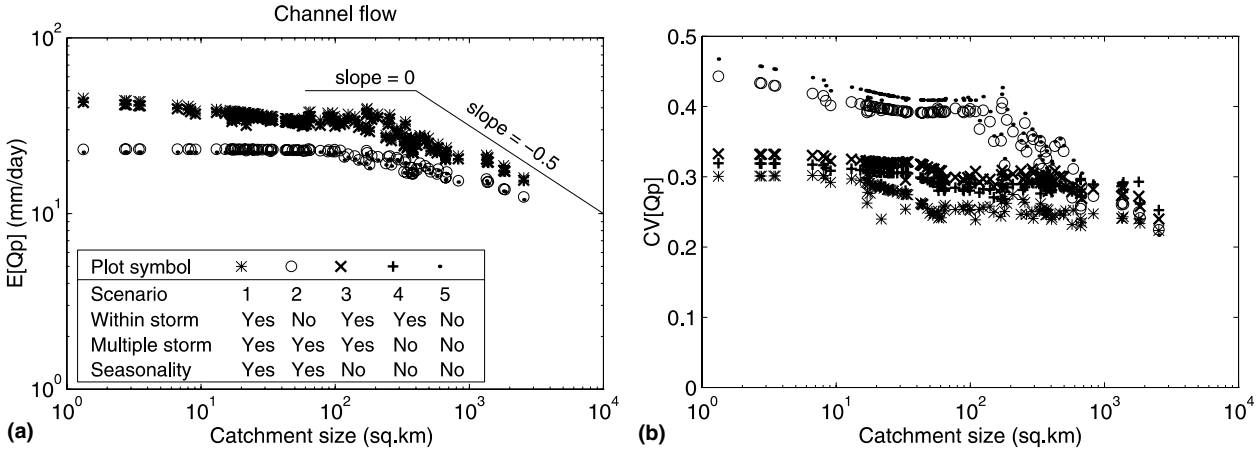

Fig. 8. (a) $E[Q_p]$, and (b) $CV[Q_p]$, as a function of catchment area for Group (i) runoff process (channel flow only), and Case I: Collie catchment.

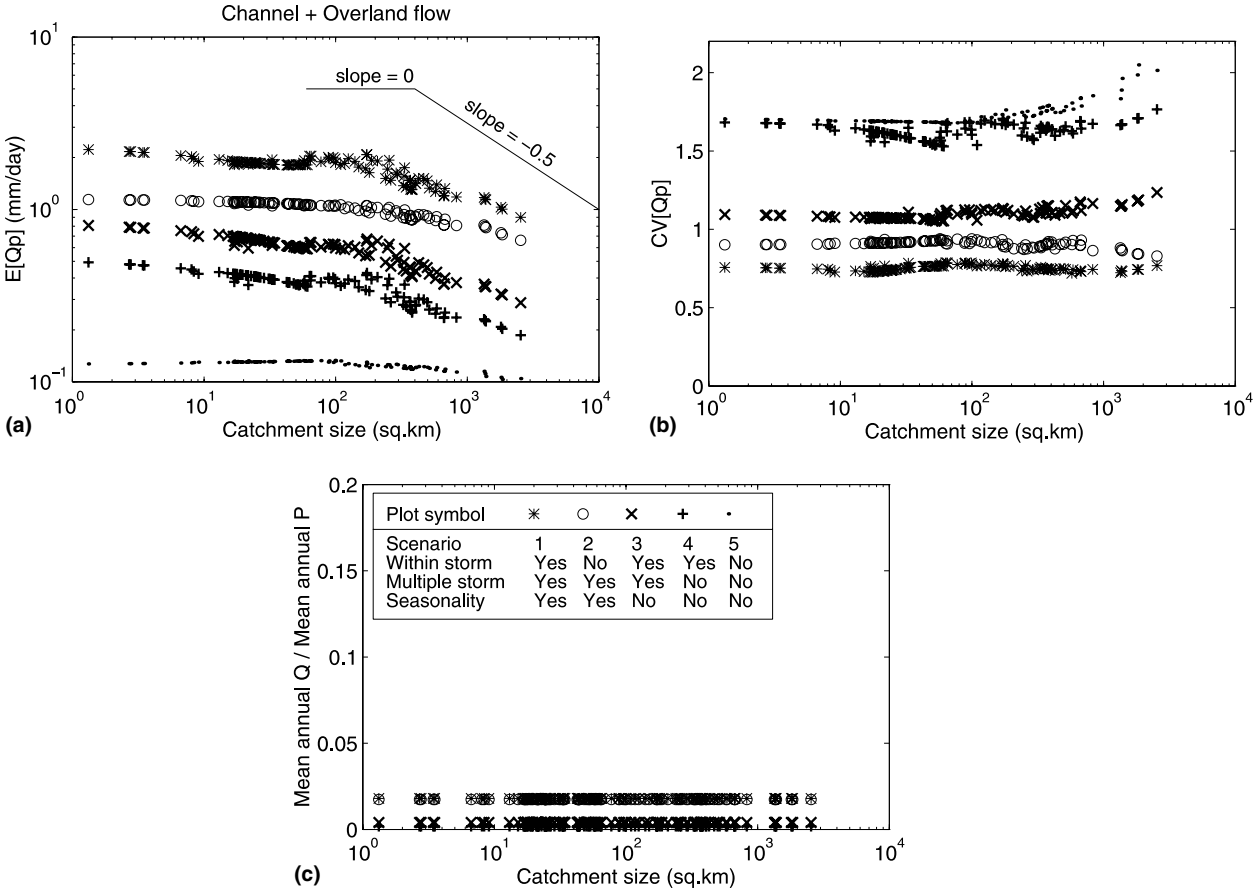

Fig. 9. (a) $E[Q_p]$ and (b) $CV[Q_p]$, and (c) annual Q/P, as a function of catchment area for Group (ii) runoff processes (channel flow and overland flow), and Case I: Collie catchment.

the inclusion of substantial evapotranspiration, with the allowance of soil water storage. The rate of decrease of θ with increasing catchment size remains roughly the same for all the rainfall scenarios, despite large differences in $E[Q_p]$ and c (Fig. 9(a)). The significant differences in both $E[Q_p]$ and $CV[Q_p]$ for the five rainfall scenarios demonstrate that all of the temporal scales of rainfall are important in the determination of flood peaks and their scaling for this combination – within-storm patterns interact with overland flow, while the longer time scales control the peak through their impacts on antecedent moisture contents. Annual water yield, on the other hand, does not vary with catchment size. This is because the input climate data

and subcatchment characteristics have been assumed to be uniform in space (Fig. 9(c)).

Fig. 10(a) shows the scaling behaviour of $E[Q_p]$ for the Group (iii) runoff process combination, namely subsurface flow and channel flow. A major change from Fig. 8(a) is the almost marginal increase of θ with increase of catchment size, which corresponds to the behaviour of a slow catchment, reported in Section 2.1 (Fig. 4(a), $t_h = 100$ h). For rainfall scenarios 4 and 5, $E[Q_p]$ and c are significantly smaller than the three scenarios which include multiple storms and/or seasonality. This shows that multiple storms and seasonality are important controls for slow catchments. On the other hand, in comparison to Group (ii) (overland flow with channel flow), the similarities are low $E[Q_p]$, high CV and low annual water yield which is below 7% of annual rainfall (Fig. 10). However, the inclusion of subsurface flow leads to differences in annual water yield between the five rainfall scenarios. This is due to the non-linearity of the subsurface flow process interacting with the accumulation of soil moisture storage when multiple storms and seasonality are allowed in the rainfall inputs. The results for Group (iv) of runoff process combinations (i.e., overland flow, subsurface flow and channel flow) are presented in Fig. 11. The results are very similar to the previous Group (iii) (Fig. 10), in terms of both magnitude and shape. This result is quite predictable since the dominant mechanism of runoff generation in the Collie catchment is subsurface flow.

A comparison between the different groups of runoff combinations is shown in Fig. 12, with plots of $E[Q_p]$, $CV[Q_p]$ and annual water yield against catchment area, for the most complete rainfall description, namely, scenario 1. Identical results for $E[Q_p]$ and the annual water yield are obtained for Group (iii) and Group (iv) confirming that subsurface flow is the dominant runoff generation process (Fig. 12(a),(c)). Fig. 12(b) also reveals that the introduction of saturation excess overland flow tends to slightly reduce the $CV[Q_p]$, as compared to Group (iv), however, in all cases the $CV[Q_p]$, tends to remain roughly constant with catchment area.

4.3.2. Case II: Collie catchment with Queensland climate

Mean annual rainfall in the Broken River catchment in Queensland is about 2100 mm, or three times higher than that of Collie catchment in Western Australia, with the mean maximum rainfall intensity also being in the

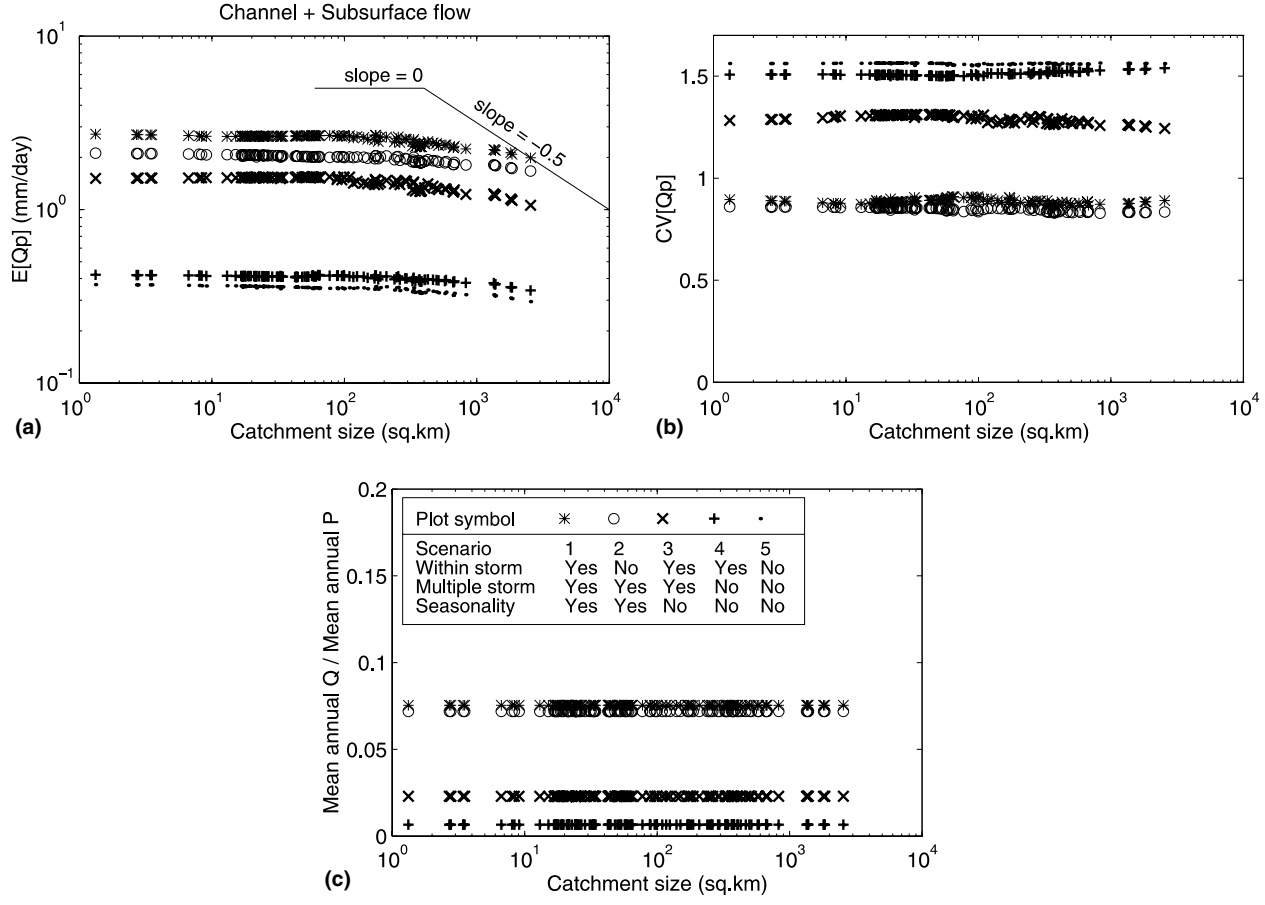

Fig. 10. (a) $E[Q_p]$ and (b) $CV[Q_p]$, and (c) annual Q/P, as a function of catchment area for Group (iii) runoff process (channel flow with subsurface flow), and Case I: Collie catchment.

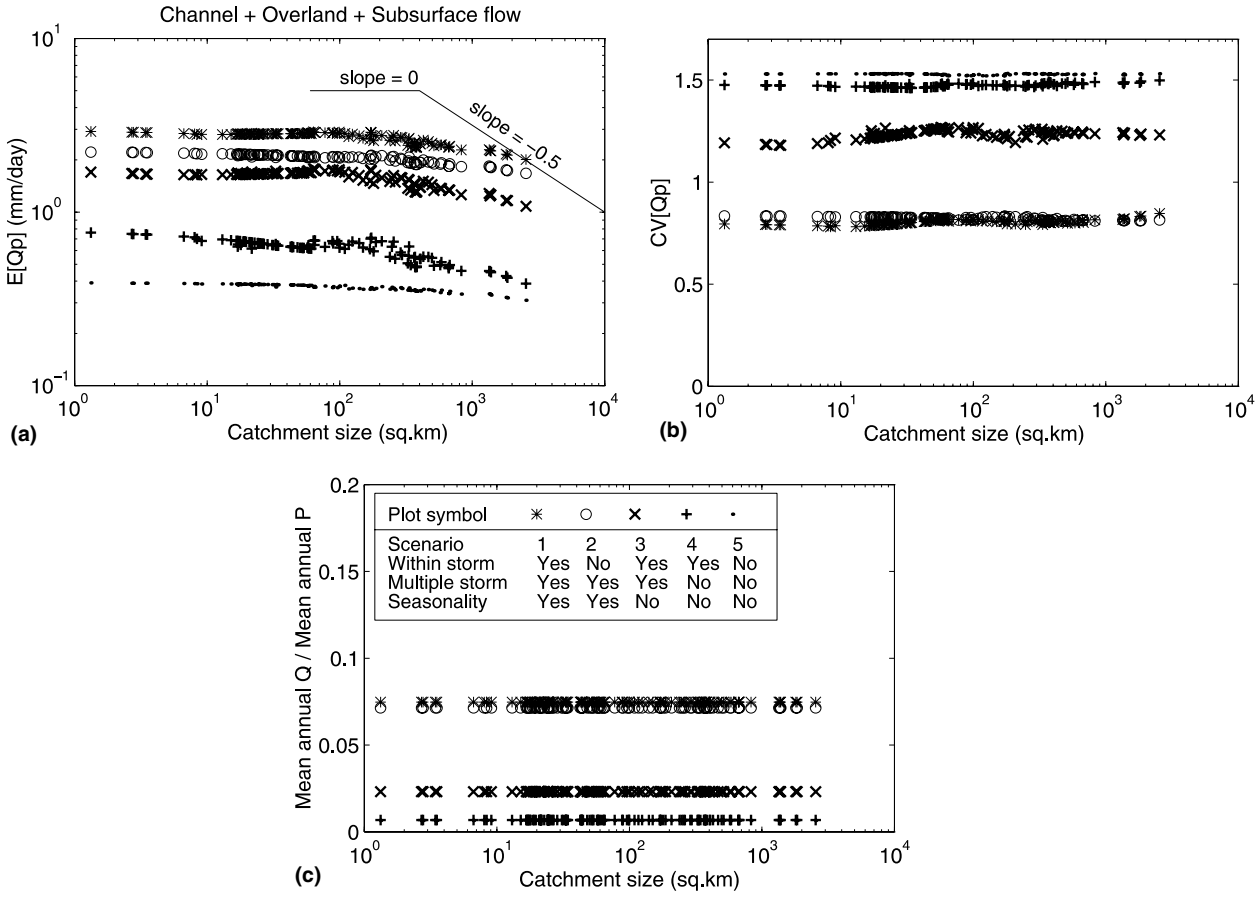

Fig. 11. (a) $E[Q_p]$ and (b) $CV[Q_p]$, and (c) annual Q/P as the function of catchment size for Group (iv) runoff process (channel flow with overland and subsurface flow), and Case I: Collie catchment.

same proportion (Table 1). Fig. 13 shows a comparison of mean monthly rainfalls between the Collie and Broken River catchments.

Fig. 14 presents the results for the five rainfall scenarios using the Group (iv) runoff process combinations (overland flow, subsurface flow and channel flow). The following differences between Cases II and I can be noted: (i) large separation between the magnitude and scaling behaviour of $E[Q_p]$ between rainfall scenarios with and without within-storm patterns; (ii) larger decrease of the scaling exponent with increasing catchment area for rainfall scenarios with within-storm patterns; (iii) much higher annual water yield; and (iv) lower average $CV[Q_p]$, and much less separation between the five rainfall scenarios. This clearly indicates that the Queensland climate tends to encourage higher amounts of surface runoff, and the resulting fast response of the catchment tends to increase the importance of within-storm patterns.

Fig. 15 repeats the results of Case II for the most complete rainfall scenario (scenario 1), and now organised in terms of the runoff process combinations (Groups (i)–(iv)). Unlike Fig. 12 (Case I, Collie) all of them show a substantial decrease of θ with catchment size. The largest separation in both $E[Q_p]$ and $CV[Q_p]$ appears when we go from Group (ii) (overland flow dominated) to Group (iii) (subsurface flow dominated), whereas a change from Group (iii) to Group (iv) makes very little difference. This confirms that as a consequence of changed water balance, catchment response is changed from being slow (Case I) to fast (Case II), caused by the non-linearity of storage–discharge relationship relating to subsurface stormflow. The values of $E[Q_p], CV[Q_p]$ and the mean annual water yield of Group (iii) and Group (iv) are almost identical, suggesting that subsurface flow is still the dominant runoff process.

4.3.3. Study Case III: Collie network with Queensland water balance

To further investigate the effect of different climate conditions and catchment characteristics, we use climate data and the soil and vegetation parameters, all taken from the Broken River catchment. In other words, we replace Collie's water balance with Broken River catchment's water balance.

Fig. 16 shows $E[Q_p], CV[Q_p]$ and annual water yield for the five rainfall scenarios plotted against catchment

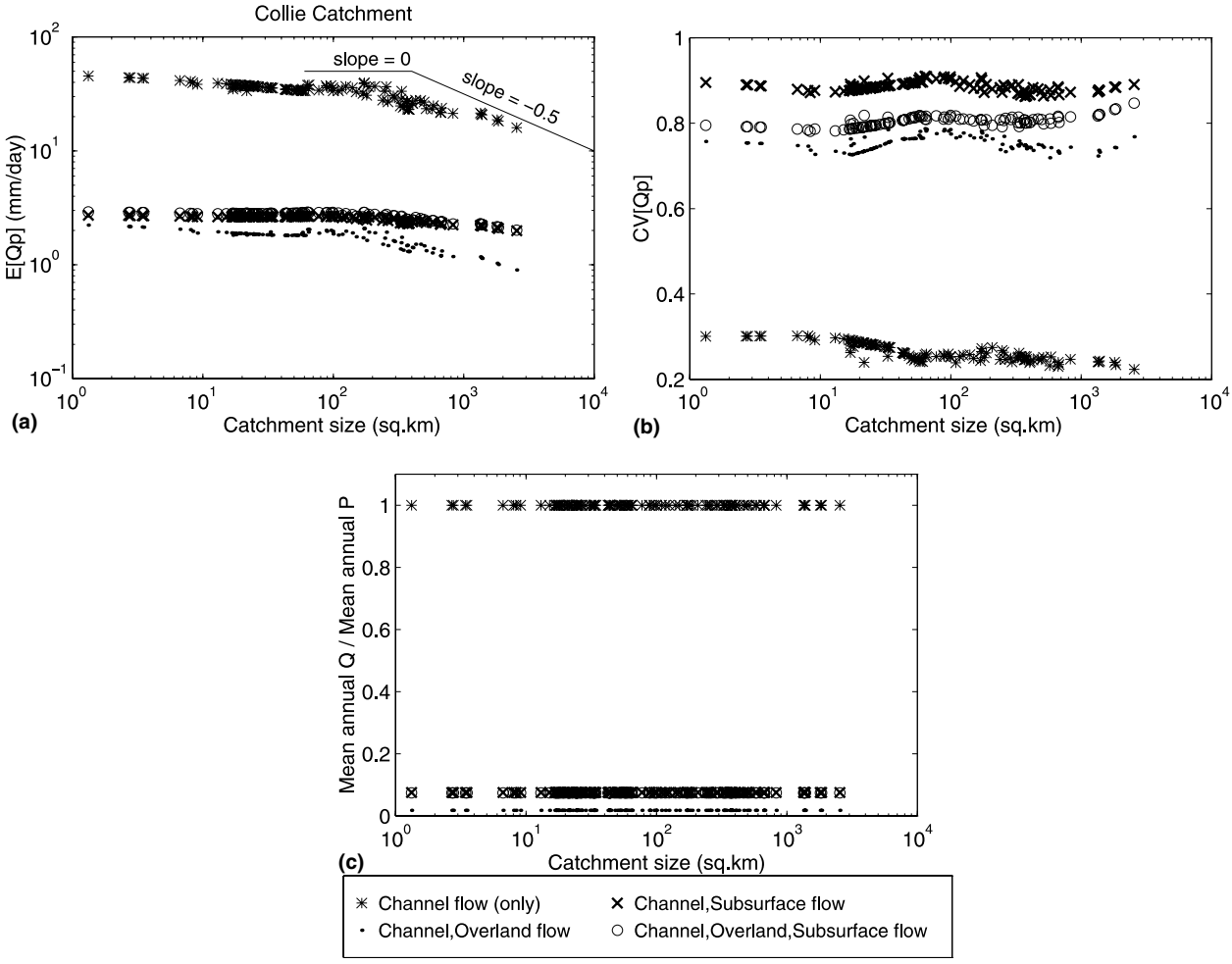

Fig. 12. (a) $E[Q_p]$ and (b) $CV[Q_p]$, and (c) annual Q/P, as a function of catchment area for runoff process Groups (i)–(iv), for rainfall scenario 1 and Case I: Collie catchment.

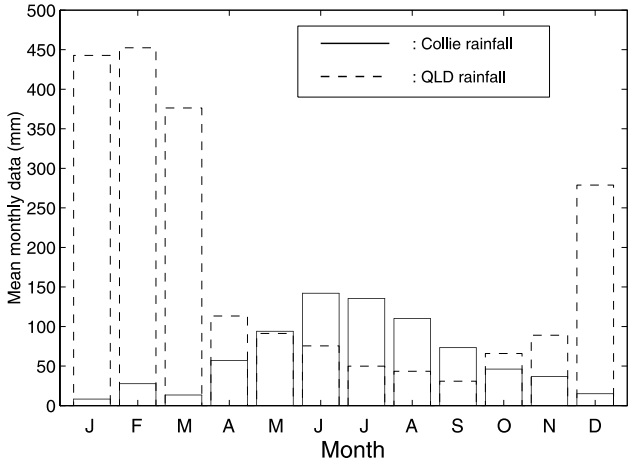

Fig. 13. Comparison of mean monthly rainfall from Collie (Western Australia) and Broken River (Queensland) catchments.

area, for the Group (iv) runoff process combination (overland flow, subsurface flow and channel flow). Comparison of the results for Case II (Fig. 14) and Case III (Fig. 16) shows that the differences are slight. This suggests that the catchment flood response is similar despite having different characteristics of hillslope water balance. Similar to Case II, catchment response in Case III can be classified as fast.

Fig. 17 presents the results $E[Q_p]$, $CV[Q_p]$ for just rainfall scenario 1, but organised in terms of the four runoff process groupings. Identical results for $E[Q_p]$ obtained for the Group (ii) and Group (iv) processes suggest that the dominant process control of flood peaks has switched from subsurface flow to overland flow (Fig. 17(a)). We attribute this change to a change in mean soil depth, from the deep soils found in Collie to shallower soils found in Broken River. However, despite this, subsurface flow remains the dominant control as far as the annual water yield is concerned in all cases (Figs. 12(c), 15(c), 17(c)).

4.4. Discussion: study Cases I, II and III

Table 3 shows a summary the results for peak flows for the Group (iv) runoff process combination for all

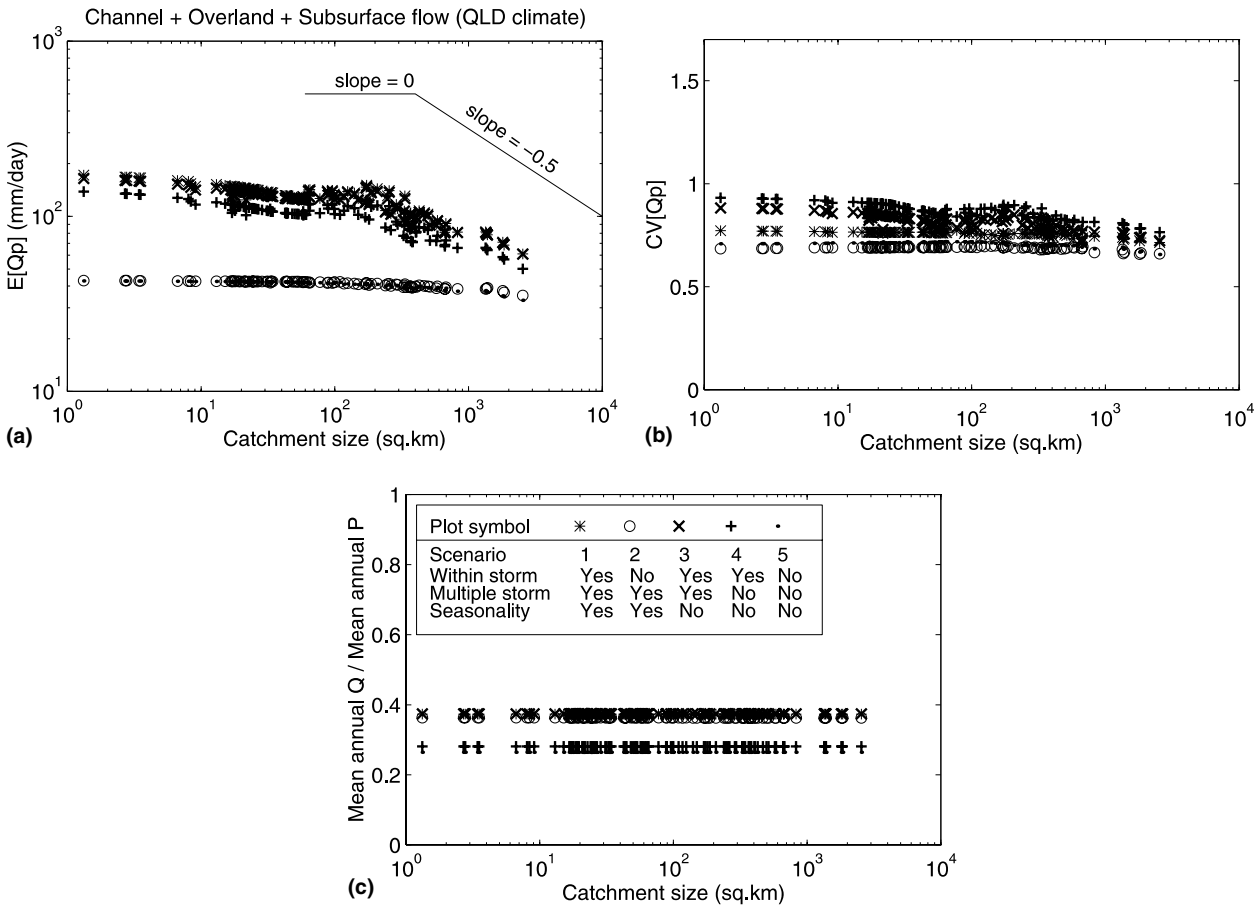

Fig. 14. (a) $E[Q_p]$ and (b) $CV[Q_p]$, and (c) annual Q/P, as a function of catchment area for Group (iv) runoff process (channel flow with overland and subsurface flow), and Case II: Collie catchment with Broken River climate.

three Cases, I, II and III. For Case I, the dominant runoff process is subsurface flow associated with the deep soils and low annual rainfall. These factors combine to give higher average θ and a narrower range of variation with catchment area ($\theta = 0$ to -0.11). With the increase of annual rainfall for the Queensland climate, as in Case II, θ is lower than for Case I, and the range of variation with catchment size considerably larger ($\theta = 0.04$ to -0.58). On the other hand, for Case III, the dominant runoff mechanism changes to saturation excess overland flow, driven by high rainfall and shallow soils. This gives a low θ and an equally wide range of variation of θ with catchment size ($\theta = 0.06$ to -0.52), as in Case II. A resonance effect between the fast runoff response and the within-storm patterns of rainfall variability may be responsible for providing lower θ in small catchments and wide range of variation of θ with catchment area, similar to the case of the hypothetical catchment considered in Section 2.

When only channel flow is included, and evaporation is ignored, within-storm patterns of rainfall intensity are the only factor that influences the scaling of flood peaks, especially for small catchments (Fig. 8(a)). This reduction, and the relative separation of the coefficient c between the five rainfall scenarios, is large when a realistic treatment of water balance is included with the inclusion of evaporation and non-linearity of runoff processes (Figs. 9(a), 10(a), 11(a)). It was also found that inclusion of increased complexity in rainfall patterns leads to larger values of c. However, the magnitude of the increase of c is different between slow and fast catchments. For example, adding multiple storms and seasonality gave a big increase for Case I (slow catchment), while the addition of within-storm patterns was the one which led to a large increase for Cases II and III (fast catchments) (Figs. 11(a), 14(a), 16(a)). On the other hand, the range of variation range of c between the two extreme rainfall patterns (scenarios 1 and 5) for Case I is larger than that for Cases II and III.

For Case I, $CV[Q_p]$ appears to behave almost in reverse to the behaviour of c; for example, the observed decrease of$c$ from rainfall scenarios 1–5 coincides with a corresponding increase of $CV[Q_p]$ (Figs. 8(b), 9(b), 10(b), 11(b)). However, it seemingly does

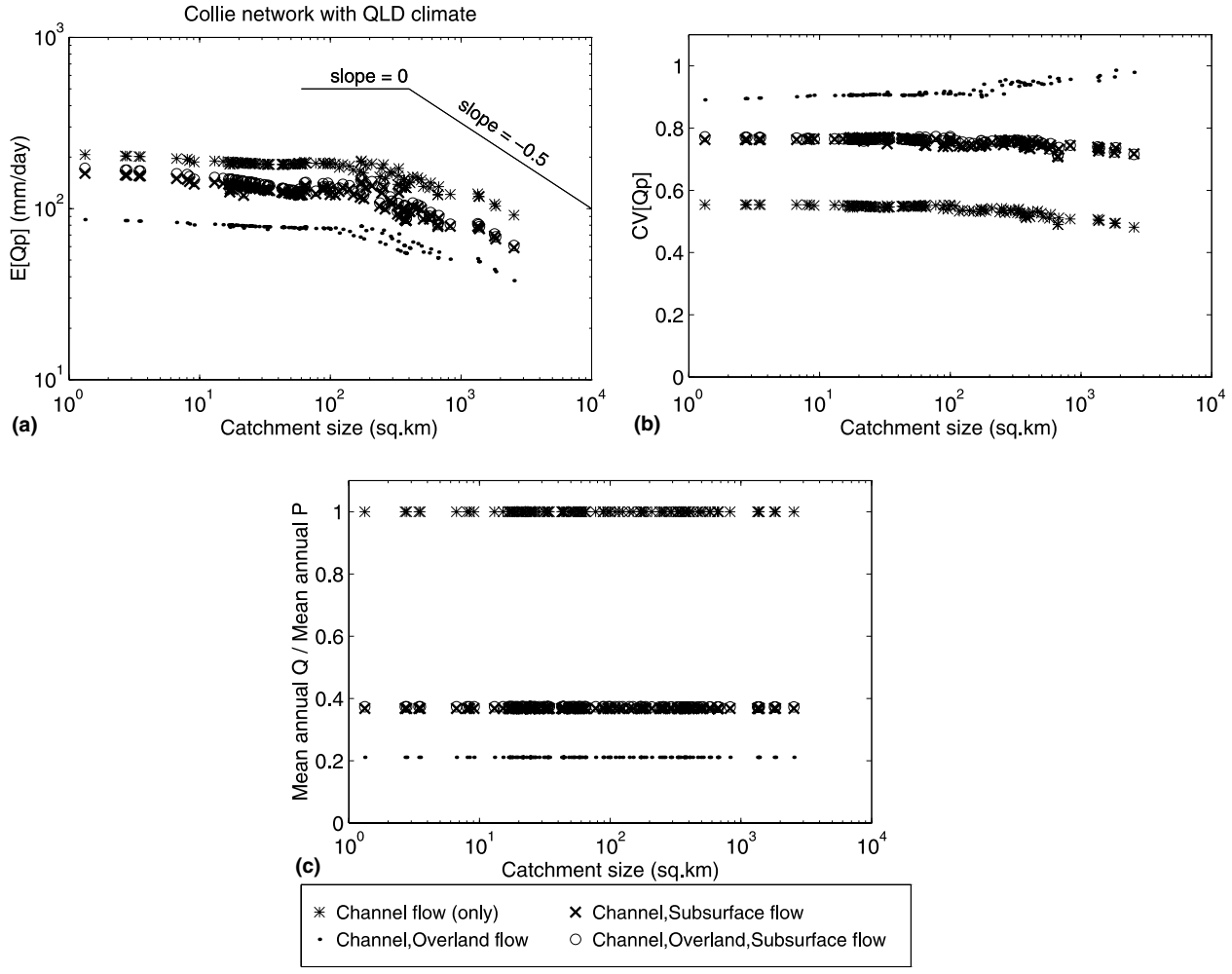

Fig. 15. (a) $E[Q_p]$ and (b) $CV[Q_p]$, and (c) annual Q/P, as a function of catchment area for runoff process Groups (i)–(iv), for rainfall scenario 1, and Case II: Collie catchment with Broken River climate.

not follow this trend for Cases II and III. In addition, for Case I when only channel flow is present, $CV[Q_p]$ is much lower than when a combination of runoff processes are present (Fig. 12(b)). However, for Cases II and III, the corresponding increase of $CV[Q_p]$ was much smaller, with a narrow range of $CV[Q_p]$ values between the various runoff process combinations (Figs. 16(b), 17(b)).

4.5. Role of catchment travel time

Water travels through a catchment system *via* different flow pathways depending on the nature of flow processes that dominate it. Constrained by the distinctive catchment characteristics (soils, topography and channel network), each runoff process has its own characteristic time scale. For example, travel times of overland flow and channel flow should be relatively shorter compared to that of subsurface flow. We use "catchment travel time" or "catchment response time" to represent the total time that water spends in the hillslopes, through overland flow and/or subsurface flow pathways, and in the river network through channel flow. In this way, we estimate total catchment travel times for the different cases looked at in Section 4.3, and the relative contributions to it from different flow processes.

Travel time between two points in the channel network can be deduced from the flow distance along the stream length and a characteristic velocity. Assuming the velocity, v, is constant in every increment of stream length Δl_i, $i = 1, 2, 3, \ldots I$ along the mainstream channel, then the travel time is given by

$$t_{ch} = \sum_{i=1}^{I} \frac{\Delta l_i}{v}. \tag{12}$$

For a catchment as a whole, the mainstream channel length is measured from the farthest point in the stream network to the outlet. Fig. 18(a) shows the mainstream

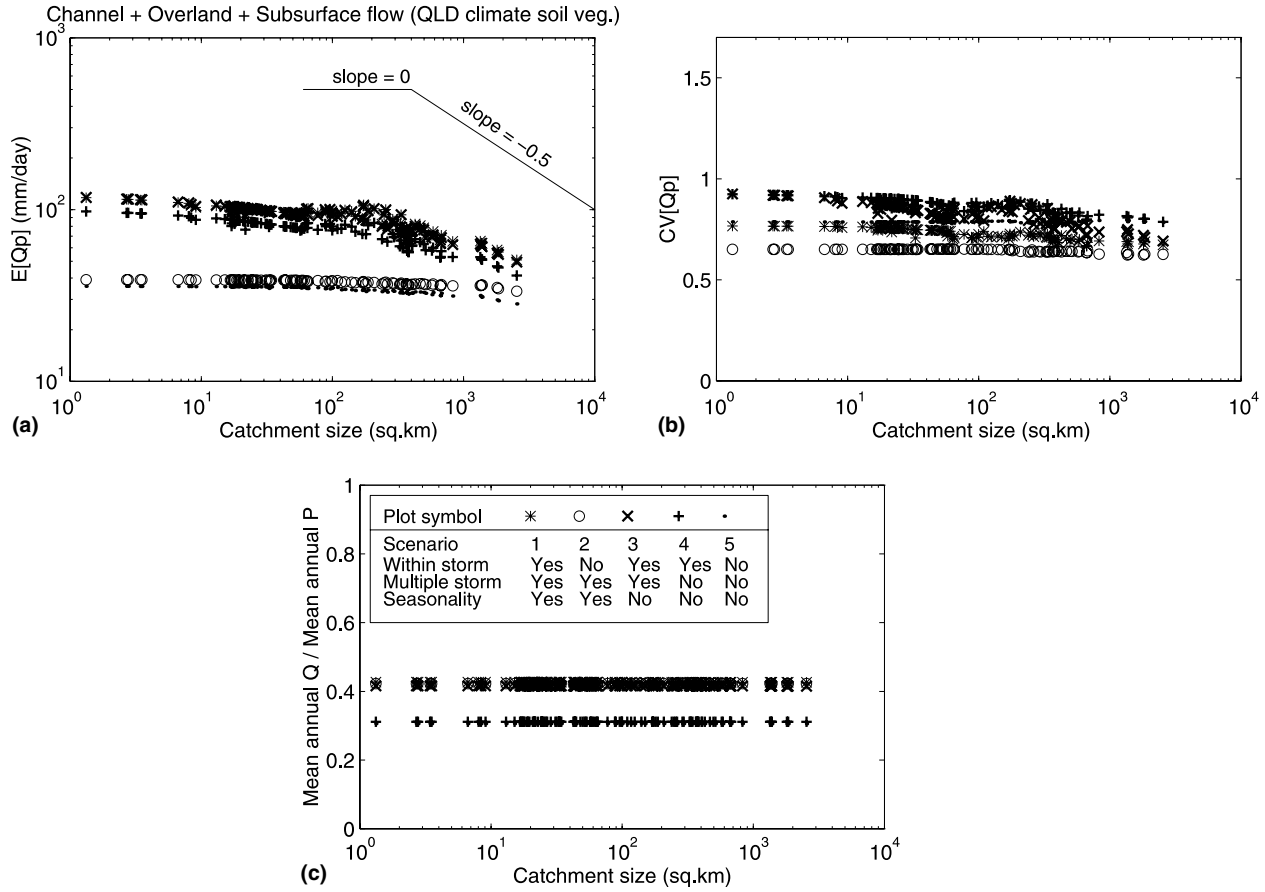

Fig. 16. (a) $E[Q_p]$ and (b) $CV[Q_p]$, and (c) annual Q/P, as a function of catchment area for Group (iv) runoff process (channel flow with overland and subsurface flow), and Case III: Collie stream network with Broken River climate, soil and vegetation.

length for the Collie catchment, and indicates that mainstream length is a power function of catchment size. The corresponding travel time in the channel network can be estimated, and is presented as a function of catchment area in Fig. 18(c).

In the hillslope water balance model, when saturation excess runoff occurs, the excess volume of water above the storage capacity is assumed to reach the stream channel within the next time step. Thus, the mean travel time of overland flow, when it exists, is approximately one day. Travel time of subsurface flow, t_s, is a function of the soil–water storage above the field capacity. It can be derived by combining Eqs. (3) and (10a) and (10b) as follows:

$$t_s = a^{1/b}(s - s_f)^{1-1/b}. \tag{13}$$

Fig. 18(b) presents the probability distributions of travel time in subsurface flow for Cases I and II for three different values of the parameter a, estimated using (13) and the probability distributions of the simulated soil–water storage. As a increases, the mean travel time in subsurface flow increases, especially substantially for the Collie catchment. Given the same parameter a, the travel time for Case II (Queensland climate) is less than that of Case I. This confirms our previous conclusion that the subsurface flow response in Collie catchment changes from slow to fast when the rainfall inputs are substantially larger, as in Queensland.

Fig. 18(c) shows a comparison of estimated travel times of channel flow (only), channel flow + overland flow, and channel flow + subsurface flow, all for Case I (Collie catchment), and the combined travel times of channel flow + subsurface flow for Case II (Collie with Queensland climate). For Case I, total catchment travel time is large, but is dominated by the slow subsurface flow in hillslopes. The consequence is that the catchment travel time is almost constant with catchment size, which is the explanation for the relative constancy of the scaling exponent of flood peaks in Collie catchment (Fig. 12(a)). For Case II, the dominance of faster subsurface flow brings the catchment travel time closer to the combination of overland flow and channel flow, which explains the considerable difference in travel times between small

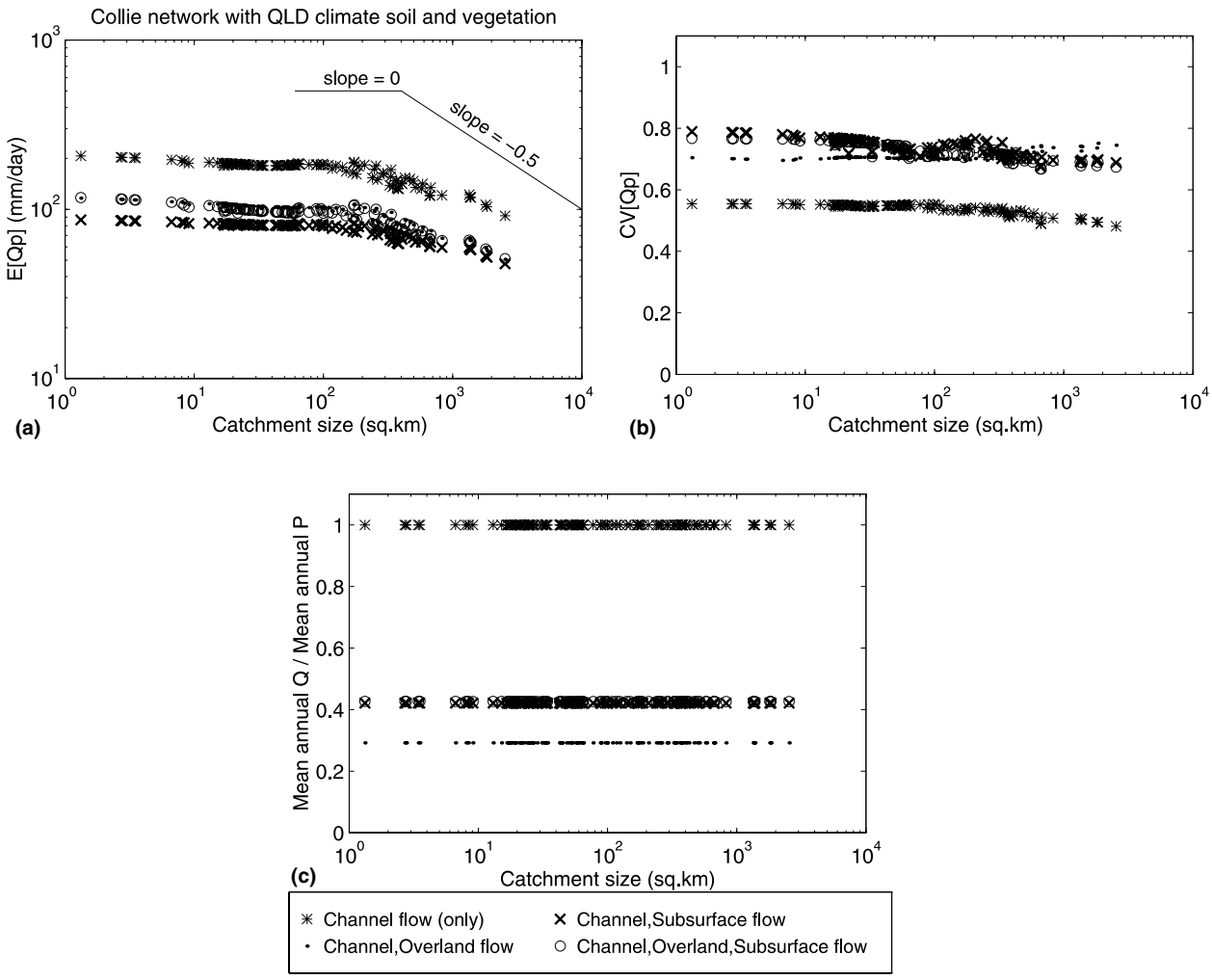

Fig. 17. (a) $E[Q_p]$ and (b) $CV[Q_p]$, and (c) annual Q/P, as a function of catchment area for runoff process Groups (i)–(iv) for rainfall scenario 1, and Case III: Collie stream network with Broken River climate, soil and vegetation.

Table 3
Summary results of peak flow simulations for three cases

	Case		
	1	2	3
Climate	Collie, WA	Broken, QLD	Broken, QLD
Subcatchment characteristics	Collie,WA	Collie, WA	Broken, QLD
Stream network	Collie, WA	Collie, WA	Collie, WA
Dominant runoff process	Subsurface and channel flow	Subsurface and channel flow	Overland and channel flow
Hydrologic regime	slow	fast	fast
Mean annual yield, Q/P	0.075	0.37	0.43
$E[Q_p]$			
min	2.00	60.94	90.52
max	2.91	171.78	206.53
θ			
min	−0.11	−0.58	−0.52
max	0.00	0.04	0.06
CV			
min	0.78	0.71	0.67
max	0.85	0.77	0.77

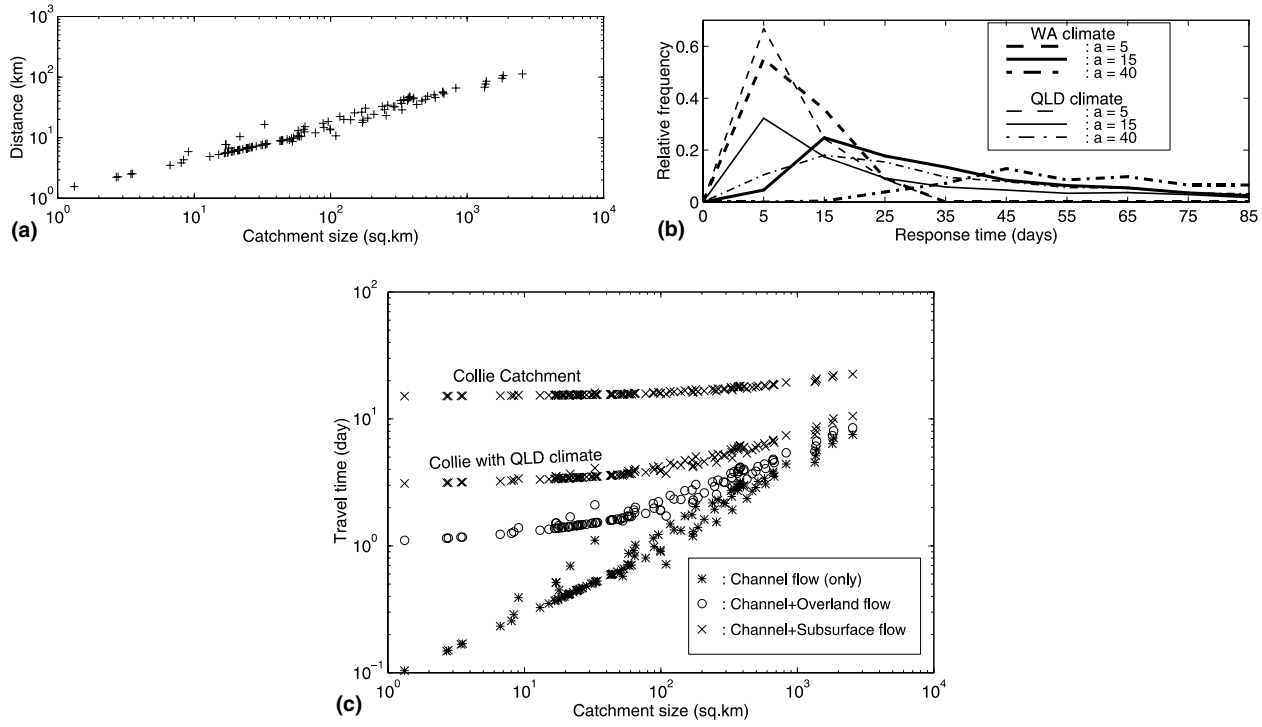

Fig. 18. (a) Measured mainstream length as a function of catchment area, (b) estimated travel times of subsurface flow pathways for different values of the non-linear storage–discharge parameter a, for Cases I and II, and (c) estimated combined catchment runoff travel times for Cases I and II.

and large catchments (Fig. 18(a)). This then explains the large decrease in the scaling exponents with increasing catchment size (Fig. 15(a)).

4.6. Effects of spatial variability of rainfall

Fig. 19 shows comparisons between the observed and simulated magnitudes of $E[Q_p], CV[Q_p]$ and the annual water yield, as a function of catchment area, for the Collie and Broken River catchments. Simulated results for the two catchments come from Cases I and III, respectively. They show a generally good match for both catchments, confirming the ability of the distributed rainfall–runoff model to capture the flood peaks and water yields, except for a slight under-estimation of $CV[Q_p]$ for the Collie catchment.

These simulation results are based on the assumption that climatic inputs and catchment characteristics are spatially uniform. Next we partially relaxed the spatial uniformity assumption for the Collie catchment, and used spatially variable climatic inputs (rainfall and potential evaporation) in the model simulations, based on measured rainfall data from 14 rain gauges and observed Class A pan distributed over the catchment, and the results are shown in Fig. 20. We found that not only the mean $CV[Q_p]$, but also the scatter around this mean, match the estimates obtained from measured flow data.

The spatial variability of rainfall also leads to an increase in the scatter of the relationships of $E[Q_p]$ and mean annual water yield with catchment size (Fig. 20). However, the average θ remains unchanged. Note that mean annual water yield tends to increase with catchment size in both the observed data and in the simulation results. This is because, in the Collie catchment, the general flow direction is from east to west, and this direction also coincides with a generally increasing trend of rainfall as well. The discrepancy between the observed data and simulation results is still relatively large, especially for small catchments. This suggests that the spatial variability of soils and vegetation must also be included to capture this observed heterogeneity. This is left for further research.

4.7. Sensitivity to water balance parameters

A summary of the sensitivity analyses carried out on annual water yield, c, θ, and $CV[Q_p]$, with respect to the water balance parameters in the Collie catchment (Case I), is given in Table 4. Annual water yield and c are sensitive, in a similar manner, to all the

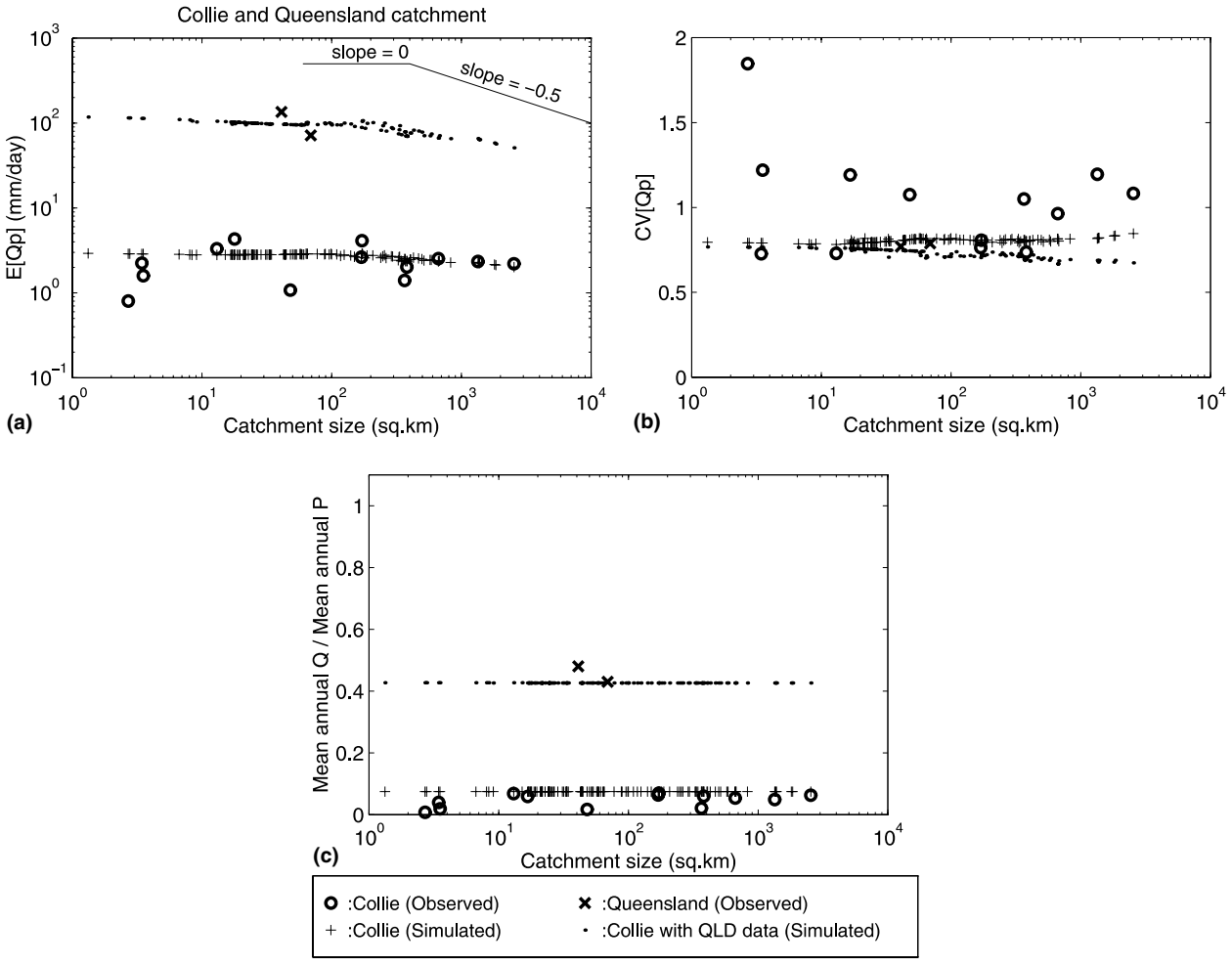

Fig. 19. Comparison of observed data and simulation results: (a) $E[Q_p]$ and (b) $CV[Q_p]$, and (c) annual Q/P as a function of catchment size, for Cases I and III.

parameters (e.g., both increase as S_b decreases), except that the annual water yield is not sensitive to a. There is no doubt that a decrease of a dictates a move towards faster catchment response, thus causing a decrease of θ. Conversely, an increase of a causes more delay in subsurface flow, and this may have the effect of altering the dominant runoff process in such a way as to increase the contribution of saturation excess overland flow. This may explain the decrease of θ, a response similar to that of a fast catchment. In general, $CV[Q_p]$ is sensitive to all parameters but tends to decrease with the increase of M and f_c, and is more sensitive to a in small catchments, than in large catchments.

5. Conclusions

In this paper, we have continued previous investigations into the physical controls on the scaling behaviour of flood peaks, and into the hypothesis that observed scaling behaviour is a reflection of interactions between time scales present in the rainfall and runoff processes. The investigation of these space–time connections is an extension of previous work of Robinson and Sivapalan [15] who used a simple linear rainfall–runoff model of a hypothetical catchment. We have carried out this investigation by considering a combination of different runoff processes. To test the ideas in actual catchments, we have used a distributed rainfall–runoff model which includes a realistic description of runoff processes, including non-linearity of runoff processes, and a simple treatment of rainfall spatial variability, both of which were ignored in the previous work Robinson and Sivapalan [15].

The distributed rainfall–runoff model consists of a hillslope water balance component and a routing component. An individual hillslope receives five possible scenarios of temporal rainfall variability, from the most complex (within-storm patterns, multiple storms and seasonality) to the most simple (independent storms of constant intensity). The hillslope allows wa-

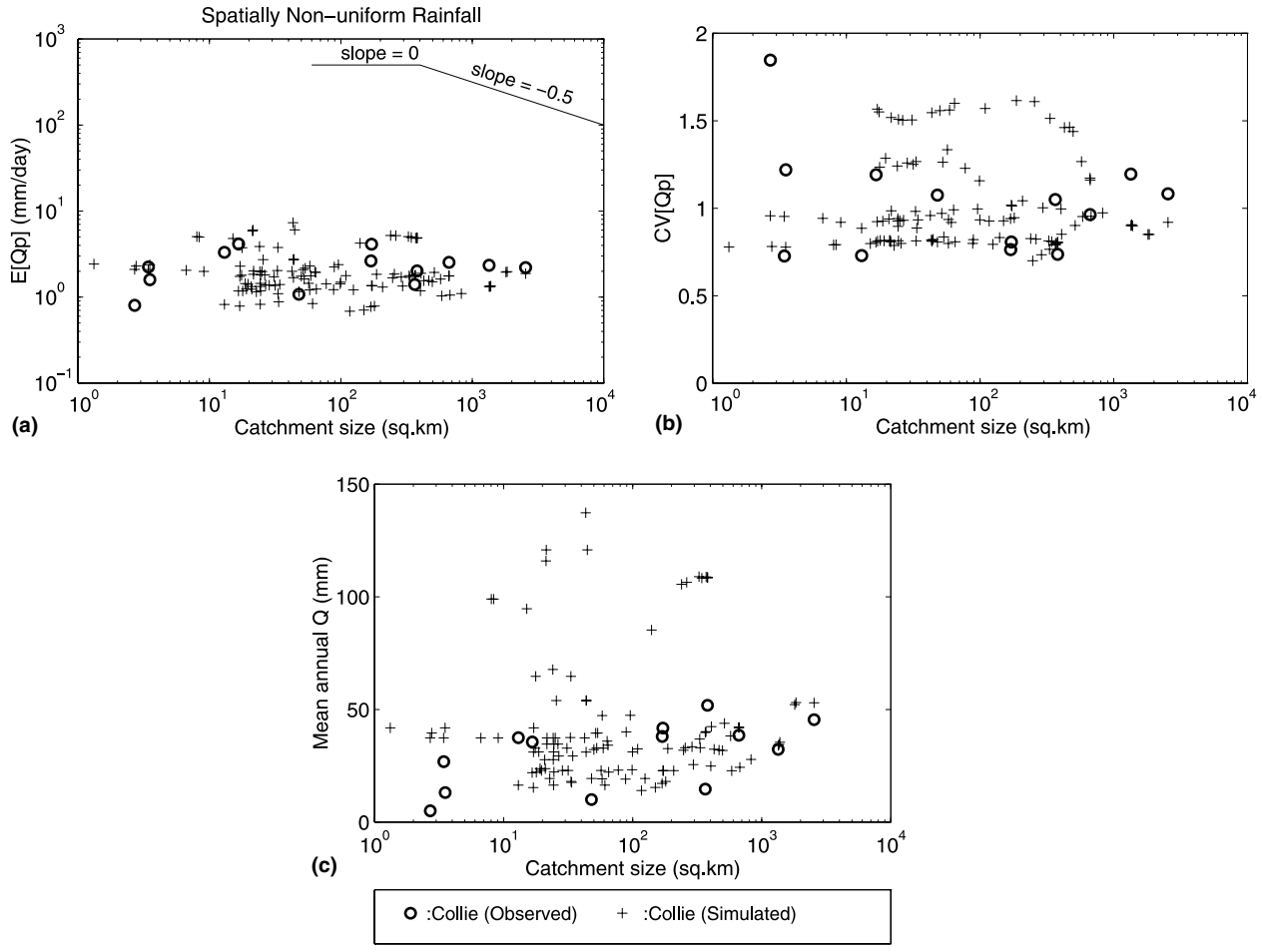

Fig. 20. Comparison of observed data and simulation results, (a) $E[Q_p]$ and (b) $CV[Q_p]$, and (c) annual Q as the function of catchment area, using measured spatially non-uniform rainfall for Case I (Collie catchment).

Table 4
Sensitivity analysis of water balance model parameters on mean annual water yield/mean annual rainfall, Q/P; constant c; scaling exponent, q; and coefficient of variation of mean annual flood peaks, $CV[Q_p]$

Parameters	Q/P	c	θ	$CV[Q_p]$
a				
↑	NS	↓	↓	↓ (small), NS (large)
↓	NS	↑	↓	↑ (small), ↓ (large)
S_b				
↑	↓	↓	NS	↑
↓	↑	↑	NS	↓
M				
↑	↓	↓	NS	NS
↓	↑	↑	NS	↓
f_c				
↑	↓	↓	↓	↓
↓	↑	↑	NS	↓

↑: Increasing; ↓: decreasing; NS: not sensitive; (small): small catchment size; (large): large catchment size.

ter to pass through it *via* three different runoff pathways: overland flow, subsurface flow and channel flow. Four possible combinations of the runoff pathways are considered, ranging from the single pathway (channel flow only), to multiple pathways with different combinations of overland flow, subsurface flow and channel flow. To investigate the effects of different climate, soil and vegetation characteristics, the model has been applied to three study cases: (i) Collie catchment, (ii) Collie catchment with Queensland climate, and (iii) Collie stream network with Queensland climate, soil and vegetation.

It was found that the dominant controls on the scaling exponent, θ, are the type of runoff process, soil depth and mean annual rainfall. The dominance of subsurface flows, deep soils, and low mean annual rainfall (Case I) give rise to a large exponent, which remains constant with area. Estimated travel times are found to be large, which supports the classification of this catchment as a slow catchment. At the other extreme, dominance of overland with shallow soils and high mean annual rainfall (Case III) gives rise to relatively smaller scaling exponents, which tend to decrease with increasing catchment area. Catchment travel time is relatively short and increases markedly with catchment

size. This type of catchment thus qualifies as a fast catchment.

The main controls on c are temporal variability of rainfall, the underlying water balance, the dominant runoff processes, soil depth and mean annual rainfall. Within-storm patterns interacting with fast runoff processes are the main controls on c for small catchments. On the other hand, for large catchments, multiple storms and seasonality interacting with slow runoff processes are the important control on c. This resembles a kind of resonance between high frequency variations of rainfall and fast runoff processes. Shallow soils with high mean annual rainfall contributes to high annual water yield, which leads to larger mean annual floods and higher c.

A general trend of the coefficient of variation of annual flood peaks, $CV[Q_p]$, is that it is larger whenever there is a multiplicity of runoff processes, as opposed to when a single process dominates (e.g., channel flow only, $CV[Q_p] \approx 0.25$–0.45), and remains equally high in both slow (Case I) and fast (Cases II and III) catchments ($CV[Q_p] \approx 0.7$–1.5). The trend of increasing $CV[Q_p]$ can be caused by multiple scaling in the combination of nonlinear runoff processes (channel flow + overland flow + subsurface flow). It suggests that the critical combination of processes that lead to the annual maximum flood peaks change with increasing return period, in such a way to cause a steepening of the flood frequency curve, and the consequent increase of $CV[Q_p]$. This result was also obtained by Robinson and Sivapalan [15] for a small catchment near the Collie catchment. Also, $CV[Q_p]$ slightly increases with catchment area, when multiple runoff processes are present, in slow catchments dominated by subsurface flow (Case I). It slightly decreases with catchment area in fast catchments (Cases II and III). Spatial variability of rainfall can lead to an increase of $CV[Q_p]$.

Although we have used data from catchments from just two different regions, our analyses have given us insights into the causes of observed spatial scaling behaviour of flood peaks, and into the relative roles of the temporal scales of variability of rainfall and runoff processes, and the effects of their spatial variabilities. The results from this work have advanced our understanding of the connections between temporal variability of rainfall–runoff processes and the spatial scaling of flood peaks in actual catchments, and the role of the underlying water balance. We believe that this understanding of the space to time connection will allow us to better interpret observed spatial scaling behaviour of flood peaks in regionalisation studies. Such analyses should be continued in many catchments, in different climatic and hydrologic settings, by including where necessary the spatial variabilities of soils and vegetation as well, to further test and verify these ideas.

Acknowledgements

This work was financially supported by a Royal Thai Government Scholarship, awarded to the first author. Additional support came from an Australian Research Council Small Grant for the work on the Collie catchment. This support is gratefully acknowledged.

References

[1] Australian Bureau of Meteorology, Benchmark stations for monitoring the impact of climate variability and change, vols. 1–7, Water Resources Assessment Section, Hydrology Branch, Melbourne, 1991.
[2] Blöschl G, Sivapalan M. Process controls on regional flood frequency: coefficient of variation and basin scale. Water Resour Res 1997;33(12):2967–80.
[3] Farmer DL, Sivapalan M, Jothityangkoon C. Climate, soil and vegetation controls upon the variability of water balance in temperate and semi-arid catchments: downward approach to hydrological prediction. Water Resour Res 2000 [submitted for publication].
[4] Gupta VK, Dawdy DR. Physical interpretations of regional variations in the scaling exponents of flood quantiles. Hydrol Process 1995;9:347–61.
[5] Gupta VK, Waymire E. Scale variability and scale invariance in hydrological regionalization. In: Sposito G, editor. Scale invariance and scale dependence in hydrology. New York: Cambridge University Press; 1998. p. 88–135.
[6] Gupta VK, Mesa OJ, Dawdy DR. Multiscaling theory of flood peaks: regional quantile analysis. Water Resour Res 1994;30(12):3405–21.
[7] Gupta VK, Castro SL, Over TM. On scaling exponents of spatial peak flows from rainfall and river network geometry. J Hydrol 1996;187:81–104.
[8] Huang HG, Willgoose G. Flood frequency relationships dependent on catchment area: an investigation of causal relationships. In: Paper Presented at Towards the 21st Century, Engineering for Water Resources Conference, Inst. of Eng. Aust., Newcastle, Australia, June 30, 1993.
[9] Jothityangkoon C. Space–time Variability and Scaling of Hydrologic Response and Role of Catchment Water Balance. PhD Thesis, University of Western Australia, Crawley, Western Australia, 2001.
[10] Jothityangkoon C, Sivapalan M, Farmer D. Process controls of water balance variability in a large semi-arid catchment: downward approach to hydrological model development. J Hydrol 2001;254(1–4):174–98.
[11] Mosley MP, McKerchar AI. Streamflow. In: Maidment DR, editor. Handbook of hydrology. New York: McGraw-Hill; 1992. p. 8.1–8.39.
[12] National Environment Research Council. Flood Studies Report, vol. 1. London, 1975.
[13] Pilgrim DH. Australia rainfall and runoff: a guild to flood estimation, vol. 1. 3rd ed. Inst. of Eng. Australia: Canberra, ACT; 1987.
[14] Robinson JS, Sivapalan M. An investigation into the physical causes of scaling and heterogeneity of regional flood frequency. Water Resour Res 1997;33(1–4):1045–59.
[15] Robinson JS, Sivapalan M. Temporal scales and hydrological regimes: implications for flood frequency scaling. Water Resour Res 1997;33(12):2981–99.
[16] Robinson JS, Sivapalan M, Snell JD. On relative roles of hillslope processes, channel routing, and network geomorphology in the

hydrologic response of natural catchments. Water Resour Res 1995;31(12):3089–101.

[17] Smith JA. Representation of basin scale in flood peak distributions. Water Resour Res 1992;28(11):2993–9.

[18] Viney NR, Sivapalan M. LASCAM: The large scale catchment model, User manual. Centre for Water Research, University of Western Australia, Report number WP 1070 NV, 1995, 199 pp.